# Late Cenozoic partitioning of oblique plate convergence in the Zagros fold-and-thrust belt (Iran)

Christine Authemayou, Dominique Chardon, Olivier Bellier, Zaman
Malekzadeh, Esmaeil Shabanian, Mohammad Reza Abbassi

## HAL Id: insu-00733486
## https://insu.hal.science/insu-00733486

Submitted on 18 Sep 2012

# Late Cenozoic partitioning of oblique plate convergence in the Zagros fold-and-thrust belt (Iran)

Christine Authemayou,[1] Dominique Chardon,[1,2] Olivier Bellier,[1] Zaman Malekzadeh,[3] Esmaeil Shabanian,[3,4] and Mohammad Reza Abbassi[3]

[1] The NW trending Zagros fold-and-thrust belt is affected by two major dextral faults: (1) the NW trending Main Recent Fault that accommodates partitioning of oblique convergence at the rear of the western Zagros and (2) the north trending Kazerun Fault located in the central Zagros. Combined structural and fault kinematics studies and SPOT images analysis have shown a Pliocene kinematic change accompanied by a fault pattern reorganization, which has led to a modification in the accommodation of oblique convergence. Since the late Pliocene, the distributed transpressional deformation operating at the rear of the belt has become partitioned along the newly formed Main Recent Fault. This fault cuts through early Pliocene nappes and transpressional structures by right-laterally reactivating high-angle thrusts. The southeastern termination of the Main Recent Fault connects to the northern termination of Kazerun Fault that consists of three fault zones that end in bent, orogen-parallel splay thrust faults. The Kazerun Fault, together with a series of north to NNW trending inherited basement strike-slip faults, define an orogen-scale fan-shaped fault pattern pointing toward the Main Recent Fault–Kazerun Fault junction. This structural pattern allows slip from along the Main Recent Fault to become distributed by transfer to the longitudinal thrust faults and folds of the Zagros belt, with the fan-shaped fault pattern acting as a horse-tail termination of the Main Recent Fault. **Citation:** Authemayou, C., D. Chardon, O. Bellier, Z. Malekzadeh, E. Shabanian, and M. R. Abbassi (2006), Late Cenozoic partitioning of oblique plate convergence in the Zagros fold-and-thrust belt (Iran), *Tectonics*, *25*, TC3002, doi:10.1029/2005TC001860.

## 1. Introduction

[2] The Zagros fold-and-thrust belt of southern Iran, the longest and widest mountain range of the Middle East Alpine orogen, currently undergoes right-oblique convergence (Figures 1 and 2). Although the structure of the Zagros results primarily from orogen-normal contraction leading to the propagation of southwest verging thrusts and folds onto the Arabian platform, two large active strike-slip fault systems affect the belt. The first one, the dextral Main Recent fault (MRF) [*Tchalenko and Braud*, 1974] runs parallel to the belt close to the suture zone and can be traced almost continuously from the triple plate junction of easternmost Anatolia to ~51°E (Figure 1) [*Talebian and Jackson*, 2002]. Together with the East and North Anatolian faults, the MRF contributes to the indentation of Eurasia in the Caucasus and anticlockwise rotation of the Arabian plate (Figure 1) [*Reilinger et al.*, 1997; *Talebian and Jackson*, 2002]. The MRF also accommodates the strike-slip component of the partitioned motion of oblique plate convergence across the Zagros [*Talebian and Jackson*, 2002]. The southeastern termination of the MRF coincides with a series of north to NNW trending, dextral strike-slip faults disrupting the structures of the belt at a high angle [e.g., *Falcon*, 1969], the most prominent of these being the Kazerun Fault (KF) (Figure 1).

[3] This paper is a contribution to the understanding of the tectonic significance of orogen-parallel and orogen-oblique strike-slip faults in collisional belts submitted to oblique plate convergence. More precisely, it aims to evaluate, in the case of the Zagros, the late Cenozoic space and time relationships between the creation of the fold-and-thrust belt and the activity of the MRF and KF strike-slip fault systems. This paper is an extension of an earlier synthetic work by *Authemayou et al.* [2005] that documented a connection between the MRF and KF, and suggested slip transfer and distribution from the MRF to the thrust ramps of the Zagros belt through the activation of the KF and associated faults.

[4] The aims of the present contribution aims are (1) to enlarge the area of investigation around the MRF, KF, and associated faults, (2) to better define the mechanisms and age of the initiation of slip along the MRF, and (3) to evaluate the consequences of the activation of this fault on the kinematic evolution of the fold-and-thrust belt, the KF, and associated faults. It is based on an integrated study

[1]Centre Européen de Recherche et d'Enseignement de Géosciences de l'Environnement (UMR CNRS 6635), Université Paul Cézanne, Aix-en-Provence, France.

[2]Now at Institut de Recherche pour le Développement, UMR 161-CEREGE, Nouméa, New Caledonia.

[3]International Institute of Earthquake Engineering and Seismology, Tehran, Iran.

[4]Now at Centre Européen de Recherche et d'Enseignement de Géosciences de l'Environnement (UMR CNRS 6635), Université Paul Cézanne, Aix-en-Provence, France.
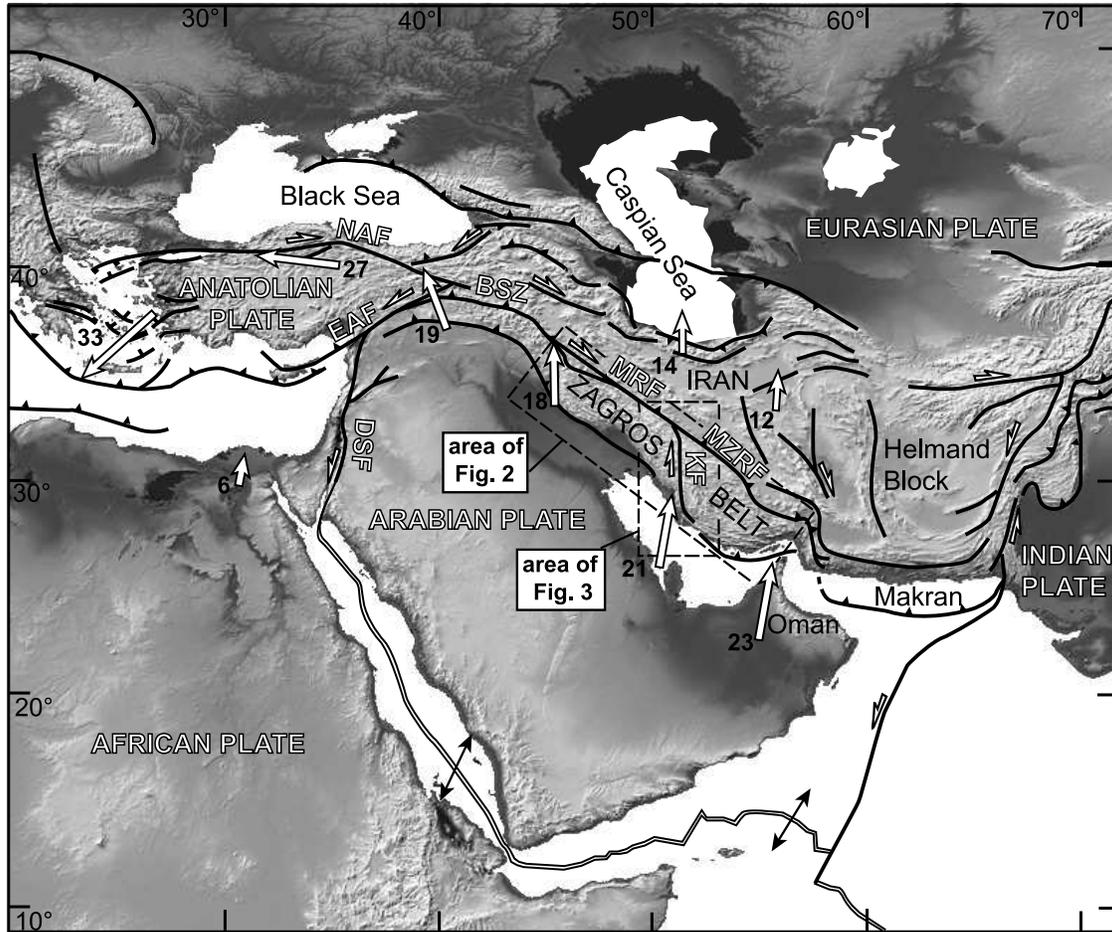
**Figure 1.** Structural frame of the Alpine collision belt in the Middle East. BSZ, Bitlis Suture Zone; DSF, Dead Sea Fault; EAF, East Anatolian Fault; KF, Kazerun Fault; MRF, Main Recent Fault; MZRF, Main Zagros Reverse Fault; NAF, North Anatolian Fault. White arrows indicate velocity vectors with respect to stable Eurasia [*Reilinger et al.*, 1997; *Vernant et al.*, 2004]. Velocities are given in mm/yr.
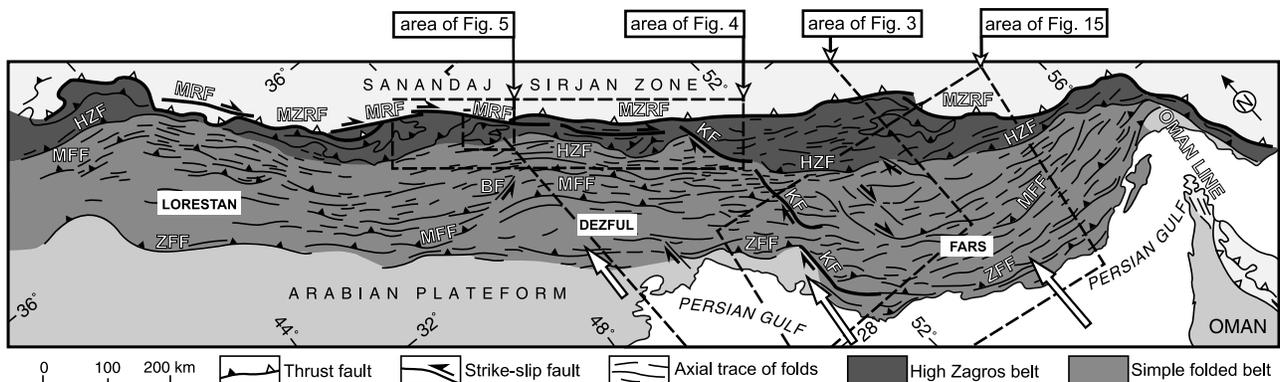


**Figure 2.** Structural map of the Zagros fold-and-thrust belt [after *Berberian*, 1995; *Sherkati and Letouzey*, 2004]. Computed shortening rates across the belt [*Vernant et al.*, 2004] are shown. BF, Balarud Fault; HZF, High Zagros Fault; MFF, Main Frontal Fault; ZFF, Zagros Frontal Fault. Lurestan, Dezful, and Fars are subdivisions of the Simple Folded Belt [*Stöcklin*, 1968; *Falcon*, 1974]. Map location is indicated on Figure 1.

combining field structural analysis, compilation of existing geological maps and data, available seismological data, SPOT and Landsat satellite images analyses and extensive fault kinematics study provided by inversions of fault slip data.

[5] We first present the results of a structural analysis and synthesis of the MRF and KF and related faults, with respect to the surrounding folds and thrusts. This analysis, complemented by fault slip data inversions, is used to investigate a reorganization of the fault pattern at the onset of right-lateral slip along the MRF during Pliocene times. This reorganization accompanied a regional kinematic change from distributed transpression at the rear of the fold-and-thrust belt to partitioning of oblique plate convergence along the MRF.

## 2. Geological Outline

### 2.1. Structure

[6] The Zagros fold-and-thrust belt stretches from easternmost Turkey to the Oman Gulf (Figure 1). At first sight, it shows a series of large longitudinal folds that affect the Phanerozoic sedimentary sequence of the northeastern Arabian margin [e.g., *Stöcklin*, 1974; *Berberian and King*, 1981; *Koop and Stoneley*, 1982]. The Main Zagros Reverse Fault (MZRF) underlines the ophiolitic suture zone between the fold and thrust belt in the strictest sense and the Sanandaj-Sirjan zone, a polyphase sedimentary/metamorphic complex that forms the southern margin of the Iranian plateau [*Stöcklin*, 1968, 1974; *Berberian and King*, 1981; *Agard et al.*, 2005] (Figure 2). Various segments of the MRF disrupt the MZRF [*Gidon et al.*, 1974a] (Figure 2).

[7] The Zagros belt is divided in two main longitudinal structural domains: the High Zagros Belt and the Simple Folded Belt [*Stöcklin*, 1968] (Figure 2). The High Zagros Belt is a zone of high topography featuring numerous, steeply NE dipping thrust faults and tectonic slices that expose old sedimentary rocks (reaching lower Paleozoic levels). The Simple Folded Belt has a lower topography and relief. It is characterized by simple "Appalachian-type" longitudinal folds associated with a few major blind thrust faults [*Berberian*, 1995], such as the Main Frontal Fault and the Zagros Frontal Fault (Figure 2). Seismic activity in the Simple Folded Belt is relatively higher than in the High Zagros Belt [*Talebian and Jackson*, 2004].

### 2.2. Tectonic Evolution

[8] The Zagros belt results from the closure of the Neo-Tethys ocean [e.g., *Haynes and McQuillan*, 1974] and subsequent collision of the Arabian plate and the central Iran microcontinents, accreted to the Eurasian plate during the Mesozoic. The timing of the suturing is controversial. It is classically considered to be Late Cretaceous in age, i.e., the age of obduction [*Berberian and King*, 1981; *Alavi*, 1994]. A recent structural study indicates that final resorption of the oceanic domain took place slightly after 35 Ma [*Agard et al.*, 2005]. *Stoneley* [1981] proposed that the collision began in the Miocene, i.e., after the Oligocene

collision along the Bitlis suture farther west [e.g., *Yilmaz*, 1993] (Figure 1). A reconstruction based on a global plate motion model by *McQuarrie et al.* [2003] suggests that the collision started around 10 Ma ago.

[9] Several stratigraphic studies provide evidence for southwestward propagation of deformation in the Zagros since Eocene times [*Hessami et al.*, 2001a; *Sherkati and Letouzey*, 2004]. The front of the belt had reached today's trace of the Persian Gulf coast by the late Miocene [*Hessami et al.*, 2001a; *Homke et al.*, 2004]. On the basis of the regional progressive, synfolding unconformity of the Upper Agha-Jari Formation of late Miocene to early Pliocene age, and the abundance and wide distribution of clastic synorogenic sediments of Plio-Quaternary age throughout the Zagros (Bakhtiary Formation), the main regional shortening phase in the fold-and-thrust belt is believed to have taken place from the late Miocene and during the Pliocene [*Falcon*, 1974; *Haynes and McQuillan*, 1974; *Stoneley*, 1981; *Hessami et al.*, 2001a; *Sherkati and Letouzey*, 2004]. This compressional phase started after shortening deformation of the Anatolian-Iranian plateau decreased became negligible at the end of the Miocene [e.g., *Koçyiğit et al.*, 2001].

### 2.3. Active Deformation and Major Strike-Slip Faults

[10] GPS measurements indicate that the Arabian and Eurasian plates converge at 21 mm/yr in the vicinity of 50°E [e.g., *Vernant et al.*, 2004] (Figure 1). This convergence rate increases eastward due to the fact that the rotation pole of Arabia lies within the eastern Mediterranean region [*Jackson and McKenzie*, 1988]. Around 50°E, a north to NNE trending shortening rate of about $7 \pm 2$ mm/yr has been recorded across the Zagros [*Vernant et al.*, 2004]. This direction is approximately 45° oblique to the strike of the northwestern Zagros and normal to the structural grain of the southeastern Zagros (Figure 2). Earthquake focal mechanisms [*Berberian*, 1995; *Jackson*, 1992; *Talebian and Jackson*, 2004] indicate that convergence obliquity is turned into reverse slip along longitudinal thrusts, and into dextral strike slip on the MRF. Nearly all earthquakes are confined to depths shallower than 20 km [*Talebian and Jackson*, 2004].

[11] Finite right-lateral offset along the MRF was estimated by *Gidon et al.* [1974a] to be ~60 km in the Dorud region. Using the offset of an Upper Cretaceous ophiolitic unit and of the major drainage, *Talebian and Jackson* [2002] obtain a value of 50 km. Assuming that the right lateral slip along the MRF was initiated 3 to 5 Myr ago, they derived a strike-slip rate of about 10–17 mm/yr. This is compatible with the estimate of 10 mm/yr of *Bachmanov et al.* [2004] based on the offset of a river valley incised into a surface of likely postglacial age. GPS measurements suggest that present slip rate of the fault may be significantly slower ($3 \pm 2$ mm/yr [*Vernant et al.*, 2004]). Several large earthquakes have been reported along the MRF, the largest one of the last century being the 1909 $M_s = 7.4$ Dorud event [*Tchalenko and Braud*, 1974].

[12] The KF and associated north to NNW trending faults (Figure 3) are inherited from a Neoproterozoic tectonic
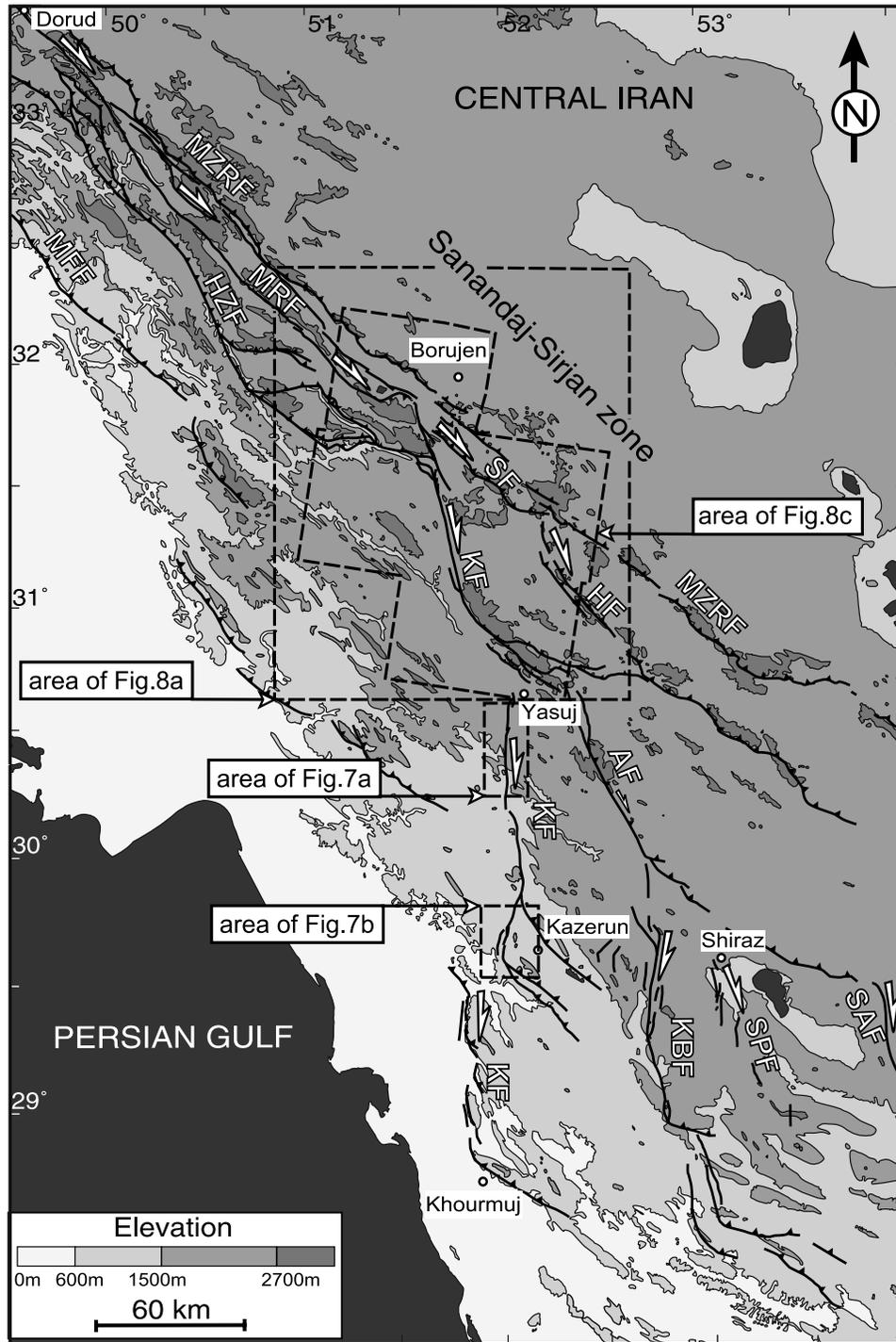
**Figure 3.** Traces of active faults in the central Zagros showing the southeastern part of the Main Recent Fault and the Kazerun Fault and associated faults (based on SPOT and Landsat images interpretation). AF, Ardakan Fault; HF, Hanna Fault; HZF, High Zagros Fault; KBF, Kareh-Bas Fault; KF, Kazerun Fault; MFF, the Main Frontal Fault; MRF, a part of the Main Recent Fault; MZRF, Main Zagros Reverse Fault; SAF, Sarvestan Fault; SF, Semirom Fault; SPF, SabzPushan Fault. Location is indicated on Figure 2.

phase [*Talbot and Alavi*, 1996; *Sepehr and Cosgrove*, 2005]. Activation of these faults probably occurred in the form of right-lateral transform faulting during Late Cambrian rifting of the Proto-Tethys and the initial stages of the Neo-Tethys rifting during the Permian [*Talbot and Alavi*, 1996] that resulted in segmentation of the Arabian margin. The KF is the longest of these faults and marks the northwestern boundary of the Fars Arc (Figure 2). It stretches from the southeastern termination of the MRF, in the north, to the Persian Gulf, in the south (Figures 2 and 3). Since the Latest Precambrian, activation or reactivation of the KF is seen in the sedimentary record [*Sepehr and Cosgrove*, 2004, 2005] as attested, for instance, by the almost exclusive occurrence of Hormuz salt within the Fars Arc [*Talbot and Alavi*, 1996].

[13] Geomorphic evidence and seismicity indicate that the KF and associated right-lateral strike-slip faults are active and affect both the cover and basement of the belt [*Baker et al.*, 1993; *Bachmanov et al.*, 2004]. Seismicity of the KF is particularly high along its central portion, where Holocene paleoearthquakes and I ≥ VIII events have been reported [*Berberian*, 1981; *Baker et al.*, 1993; *Berberian*, 1995; *Bachmanov et al.*, 2004].

# 3. Fault Pattern and Structural Analysis

## 3.1. Main Recent Fault and High Zagros Belt

[14] We studied the relations between the MRF and other structures of the High Zagros Belt between ∼49 and 52°E (Figure 4). In the northwestern part of the study area, the MRF consists of three ∼100- to 130-km-long segments that slightly overlap in the vicinity of Sahneh and Borujerd (Figure 4). The southeasternmost segment (Dorud segment) splits around 49°30′E into two 180-km-long segments, 15 km apart. These two segments merge near the southeastern termination of the MRF. In the map shown in Figure 4, two structural domains have been distinguished in the High Zagros Belt.

### 3.1.1. Domain 1

[15] In domain 1, the MRF cuts across two piled-up thrust sheets, bounded by a lower Miocene unconformity (Figure 4b) [*Braud*, 1970; *Mohajjel and Fergusson*, 2000; *Agard et al.*, 2005]. The older nappe was established from the Late Cretaceous to the Eocene [*Gidon et al.*, 1974b]. During the Miocene and the Pliocene, a second-generation nappe (Figure 4b) overthrust the High Zagros toward the SW [*Gidon et al.*, 1974c; *Agard et al.*, 2005].

[16] South of Dorud, the nappe rests on lower Pliocene conglomerates (Figures 4 and 5). Near the MRF, south vergent thrusting has taken place along the E-W trending southern boundary of the nappe [*Gidon et al.*, 1974c]. E-W to WSW trending, southerly verging ramp anticlines are observed and affect the northeastern contact between the nappe and the Pliocene basin (Figures 4 and 5). The southern front of the nappe is sealed by upper Pliocene deposits (Figures 4 and 5), indicating that southward nappe emplacement and folding stopped in the early Pliocene [*Gidon et al.*, 1974c]. All these observations are consistent with pre-late Pliocene nappe establishment, synnappe to

postnappe reverse faulting and folding having taken place in response to N-S shortening over a 25-km-wide deformation belt running parallel to, and south of, the MRF (Figure 5).

[17] In the vicinity of Dorud, both the thrust-fold system described above and the nappe are cut by a reverse fault running south of, and parallel to, the MRF. This reverse fault is in turn cut by the MRF (Figures 4 and 5). This indicates that slip along the MRF started in the late Pliocene. Dextral movement along the MRF is consistent with the shortening direction recorded by the pre-late Pliocene thrusts and folds described above.

### 3.1.2. Domain 2

[18] In domain 2, the clear-cut boundary between the Sanandaj-Sirjan zone and the High Zagros Belt is marked by the MZRF. The southern front of the belt coincides with the High Zagros Fault (HZF), which runs from the area where the MRF splits toward the southeast.

[19] The unconformity between the Eocene-Oligocene deposits and Upper Cretaceous sediments within domain 2 [*Zahedi et al.*, 1993] indicates orogenic movements during the Paleocene, the period corresponding to early nappe establishment documented in domain 1. A foreland basin initiated during the Eocene at the front of the HZF [*Hessami et al.*, 2001a; *Sherkati and Letouzey*, 2004; *Sepehr and Cosgrove*, 2004] indicates that this thrust was already active at that time.

[20] The belt is cut by a series of imbricate high-angle thrusts trending N45°E to N135°E and that were active after the Eocene (Figure 4). Thrusts lying immediately to the south of the MZRF are SW dipping, whereas thrusts closer to the HZF are preferentially NE to north dipping. Oblique, south verging thrusts are also seen SW of Ardal (Figure 4). This doubly vergent high-angle thrust system located south of the MZRF and bounded to the SW by the HZF widens eastward and becomes thinner close to the KF. This belt has the characteristics of a right-lateral transpressional flower structure. The HZF has exhumed deeper rocks as old as Paleozoic in its hanging wall, suggesting the transpressional belt (Figure 4b) is asymmetrical. Backtiary Formation conglomerates, unconformable on the Eocene to Miocene folded deposits, are cut by the HZF and internal thrusts in the High Zagros Belt. This indicates that these faults were still active and that the belt was still being thrust upon the Simple Folded Belt during the Pliocene (cross section CD; Figure 4).

[21] The southern fault zone of the MRF reuses thrust faults of the transpressional belt. In the northwestern part of domain 2, it has reactivated the main SW verging thrust located within the belt, where it mimics the NE verging northeastern boundary thrust of the belt in the southeastern part of the domain. With the MRF, the HZF is the only fault to show significant activity in the High Zagros. Microseismicity surveys [*Yamini-Fard*, 2003; *Yamini-Fard et al.*, 2006] indicate partitioning between the MRF and the HZF with depth (Figure 4, cross section EF). Reverse-slip focal mechanisms are confined to depths greater than 14 km along a NE dipping décollement, whereas dextral strike-slip focal mechanisms are recorded at shallower depths under the traces of the MRF. Map relations suggest that the
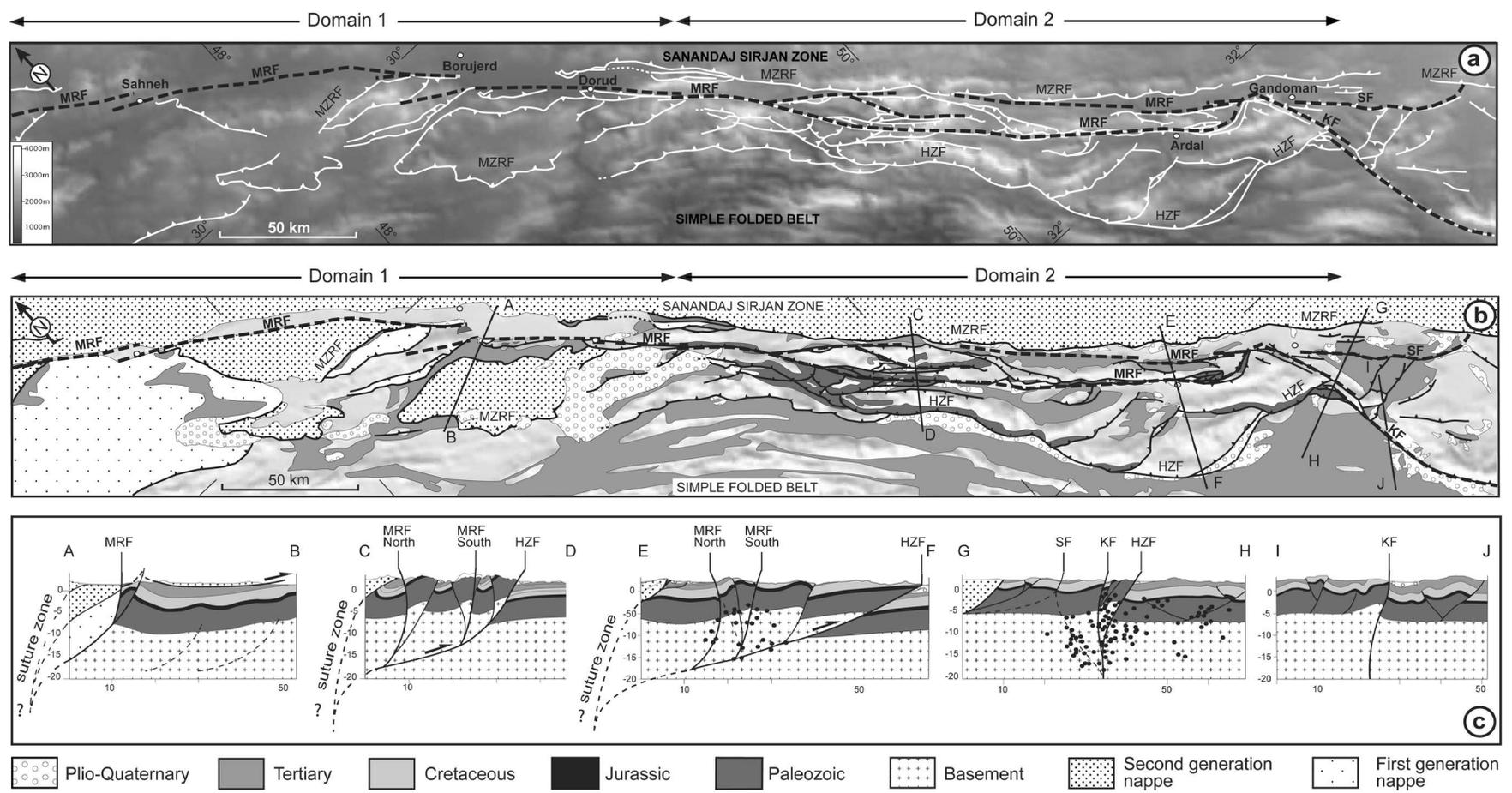
**Figure 4.** Geology and structure of the High Zagros Belt between 47 and 51°E. (a) Fault pattern superimposed on SRTM90 digital topography. Dashed lines indicate the main active faults. (b) Geological map and (c) corresponding cross sections (distances are in kilometers). Black dots are hypocenters relocated by *Yamini-Fard et al.* [2006]. Information based on SPOT and Landsat images interpretation, our field observations and a compilation of geological maps and previous works [*Braud*, 1970; *Gidon et al.*, 1974a, 1974b; *Mohajjel et al.*, 2003; *Agard et al.*, 2005; *Hajmolla-ali et al.*, 1991; *Zahedi et al.*, 1993; *Berthier et al.*, 1974; *Alavi et al.*, 1996; *Sedaghat et al.*, 1997; *Sedaghat and Shaverdi*, 1997; *Hever*, 1977; *Sedaghat and Gharib*, 1999, *Sedaghat et al.*, 1999; *Ehsanbakhsh Kermani*, 1996].
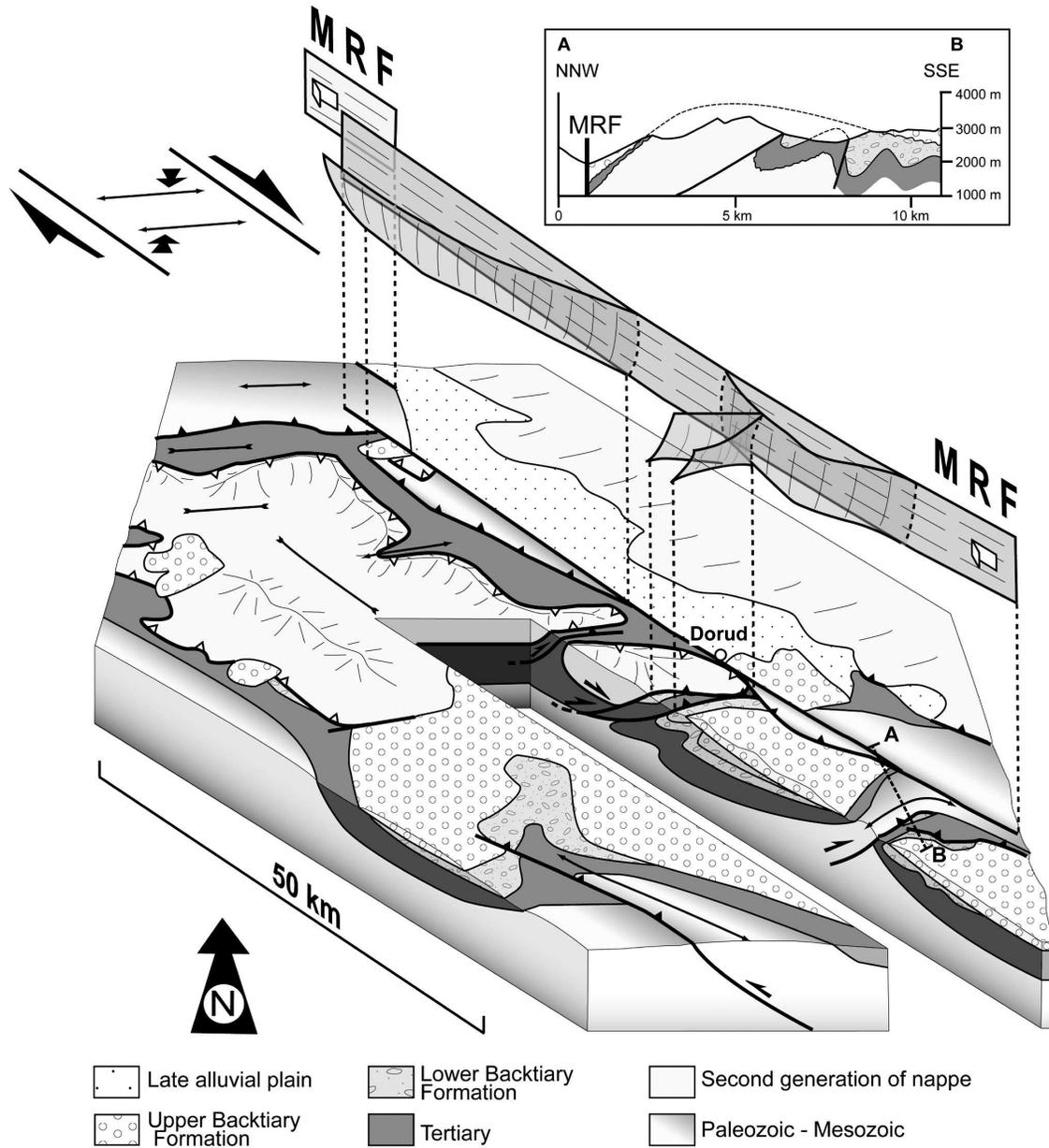
**Figure 5.** Block diagram showing the structural relationships in the Dorud region, based on mapping by *Gidon et al.* [1974c] and this study. Cross section A-B is drawn after *Berthier et al.* [1974]. See discussion in the text.

décollement corresponds to the HZF (cross section EF; Figure 4).

### 3.1.3. Tectonic Implications

[22] From Miocene to early Pliocene times in the High Zagros Belt, while nappe emplacement and N-S shortening within a NW trending shear belt was taking place around the future MRF in domain 1, a transpressional thrust belt was active in domain 2 (Figure 6). Although partitioning may already have operated along the trace of the future MRF, at least part of the strike-slip component of convergence in domain 1 must have been accommodated outside the High Zagros Belt, for example, in the Sanandaj-Sirjan

zone [e.g., *Mohajjel et al.*, 2003; *Agard et al.*, 2005]. By the early late Pliocene, deformation became partitioned along the MRF that had cut through the nappes in domain 1, right-laterally reactivated longitudinal faults of the transpressional belt (for the southwestern fault zone) and propagated south of the MZRF (for the northeastern fault zone) (Figure 6). Once cut by the MRF, the MZRF ceased to be active [*Gidon et al.*, 1974a]. The change from distributed to partitioned transpression in the High Zagros Belt led to the present-day configuration with the dextral strike-slip component of convergence taken up by the southeasternmost portion of
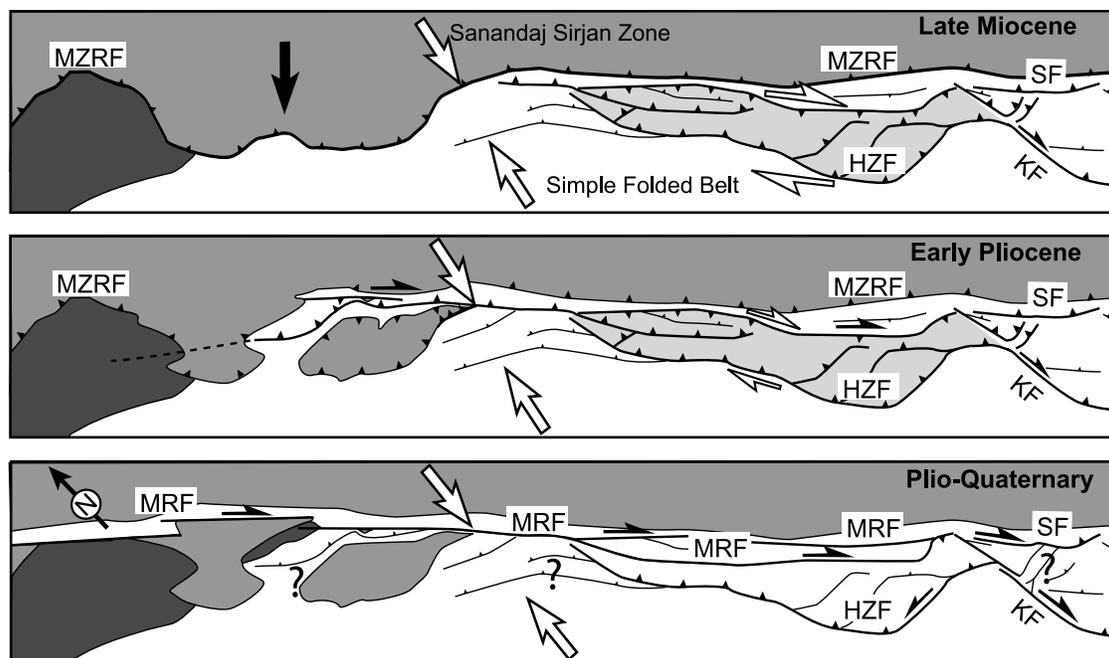
**Figure 6.** Three-stage, Late Cenozoic evolution model of the High Zagros Belt. Plate convergence vectors (white arrows) are from *McQuarrie et al.* [2003] and *Vernant et al.* [2004]. Black arrow indicates the motion of the nappes. See discussion in the text.

the MRF and the orogen-normal component of convergence accommodated by the HZF.

## 3.2. Kazerun Fault and Related Faults

### 3.2.1. Geometry

[23] The KF is composed of three north trending fault zones of equivalent length (~100 km long) (Figure 3) [*Authemayou et al.*, 2005]. They have similar trace shapes with a general N170–180°E trend and southern termina-tions bent toward SE strikes. Their terminations spilt as bend splays and are generally connected eastward to the NW trending thrust and ramp anticlines. The forelimbs of these folds are systematically overturned close to the KF and/or refolded into a knee fold, implying an increase in south verging reverse slip and/or reactivation of the ramps toward the KF. SSW of Khourmuj, bending of a large coastal anticline suggests the presence of a hidden, north trending prolongation of the southern segment of the KF reaching at least as far as the coast (Figure 3).

### 3.2.2. Total Lateral Offset

[24] The lack of piercing points and the few fold offsets induced by the KF make it difficult to establish the precise accumulated offset along the KF. Previous estimates range from 5 km (fold offsets [*Pattinson and Takin*, 1971]) to 140 km (offset of the Zagros Frontal Fault [*Berberian*, 1995]; Figure 2). The later hypothesis is questionable as the Zagros Frontal Fault may not have originally been a continuous, rectilinear structure. A new attempt has been made focusing on the central Kazerun fault zone, which exposes the clearest relations between the folds and the fault trace.

[25] On the northern part of the central fault zone (Figure 7a), anticline axial traces and bedding traces appar-ent offsets are of 1.2 to 9.2 km, assuming that faulting postdates folds with a initial NW trend. This range is in agreement with an estimate of 8.2 km of right-lateral offset, derived from the restoration of the fold topography that may be correlated from either side of the fault segment (Figure 7a). The NNW trending anticline associated with the southern thrust termination of the central fault zone is bent over a distance of 11.5 km against the north trending fault; a piece of the fold is even shifted at least 12 km northward (Figure 7b). Considering a total length of 50–65 km and a NW original trend for the anticline (i.e., the fold trend away from the fault), the cumulative right-lateral fault displacement is of the order of 22–23 (case I) or 22–27 km (case II) depending on the relative timing of folding and strike-slip-induced anticlockwise rotation of the fold. If strike slip is considered to postdate rotation and bending of the fold, the total horizontal offset is reduced to 12 km, i.e., offset of the piece of the fold (Figure 7b, case III).

[26] These results illustrate the difficulty in assessing the total lateral offset of the fault due to the complex evolution of folding, especially in the vicinity of strike-slip fault segments. Contrasted fold evolution on either side of the KF is controlled by significant sedimentary facies changes [*Sherkati and Letouzey*, 2004], out-of-sequence reactivation, and the synchronicity of folding and strike-slip movements, suggesting an independent evolution of folds on either side of the fault. Nevertheless, the north to NNW trending strike-slip segments of the central KF appear to have acted as a
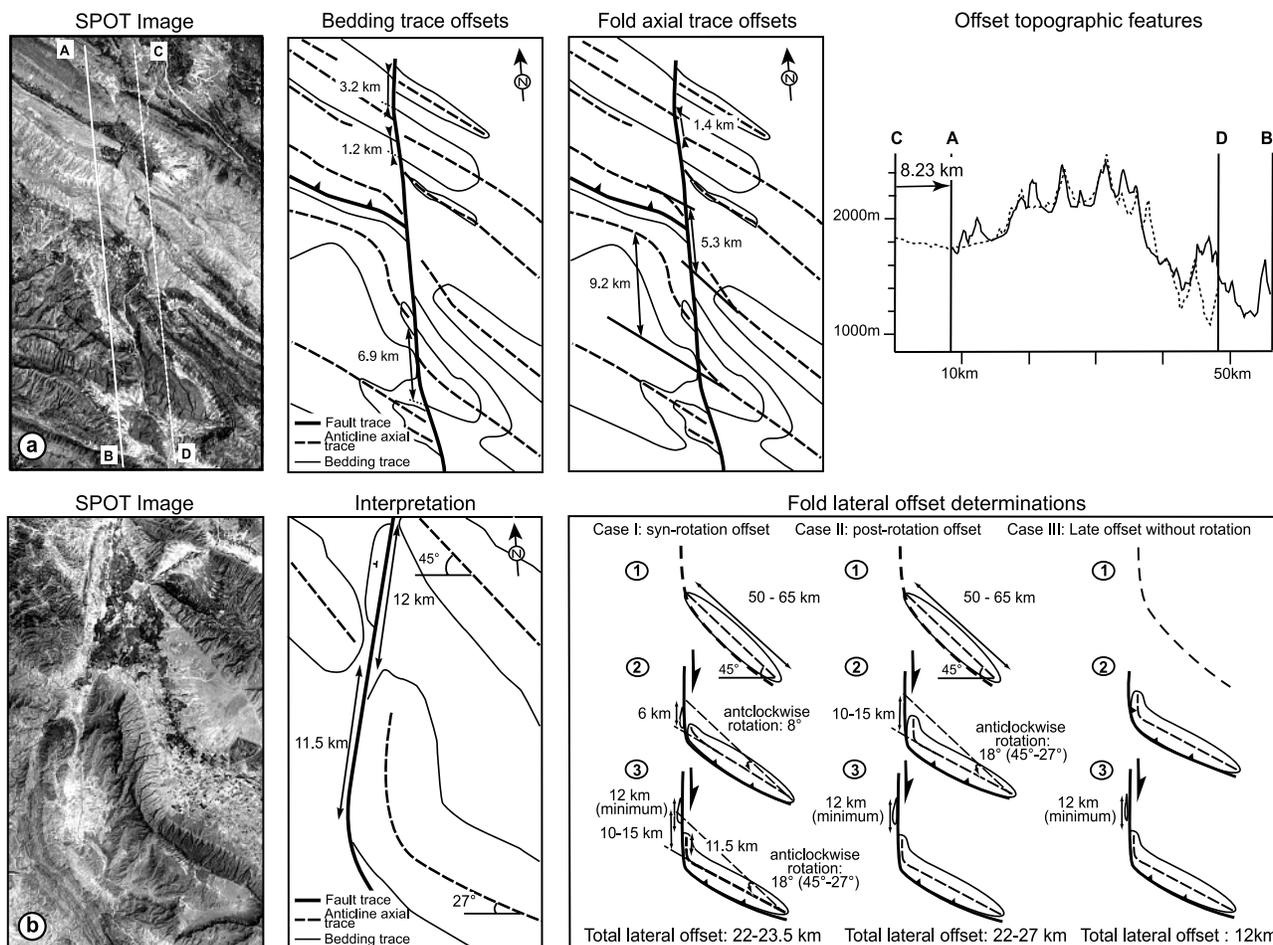
**Figure 7.** Relations between folds and the central Kazerun fault zone and lateral offsets determination. (a) Northern part of the fault zone; (b) southern part of the fault zone. In Figure 7a, the offset of the fold transversal topography on either side of the fault is obtained by restoring 8.2 km of right lateral displacement providing the best fit between topographic profiles AB and CD.

dominantly transcurrent fault, along which a minimum of 8 km of right-lateral slip may be reasonably inferred.

### 3.2.3. Related Faults

[27] Other north to NNW trending strike-slip faults in the central Zagros define, together with the KF, an orogen-scale fan shaped fault pattern that points toward the southeastern termination of the MRF [*Authemayou et al.*, 2005] (Figure 3). The faults have traces similar to that of the KF. They define a network of dominantly dextral strike-slip fault zones with orogen-parallel thrust fault terminations (Figure 3), northern or northwestern fault zone tips are systematically located close to a thrust termination.

### 3.3. Northern Tip of the Kazerun Fault in the High Zagros Belt

#### 3.3.1. Fault/Fold Pattern

[28] The rectilinear MZRF marks the northern boundary of the interaction zone between the fan-shaped fault pattern, the MRF and the HZF (Figure 8). The northern Kazerun fault zone consists of two segments. The relay zone between

these segments coincides with the area where the NW trending HZF merges with the KF (Figure 8). At its southeastern tip, the MRF gives way through a narrow discontinuity to the NNW trending northern Kazerun fault zone and to the NW trending Semirom Fault that bound the fan-shaped fault pattern described above.

[29] These two faults define a wedge-shape structural domain (Figure 8b). The region close to the vertex of the wedge, NW of Semirom, displays a series of NE trending, SE verging thrusts and folds that are cut by the Semirom Fault (Figures 8a and 8b). These thrust faults are bent terminations of the northern segment of the northern KF. They have the same orientation as those described within the transpressional belt farther west, which connect to the HZF (section 3.1.2 and Figure 4). The southern part of the wedge shows dominantly orogen-parallel folds and minor faults that are deflected toward northern trends in the vicinity of the Semirom Fault (Figure 8b).

[30] Faults in the study area have been active since at least the early Miocene, with the development of a foreland and/or piedmont basin against the Dinar thrust [e.g.,
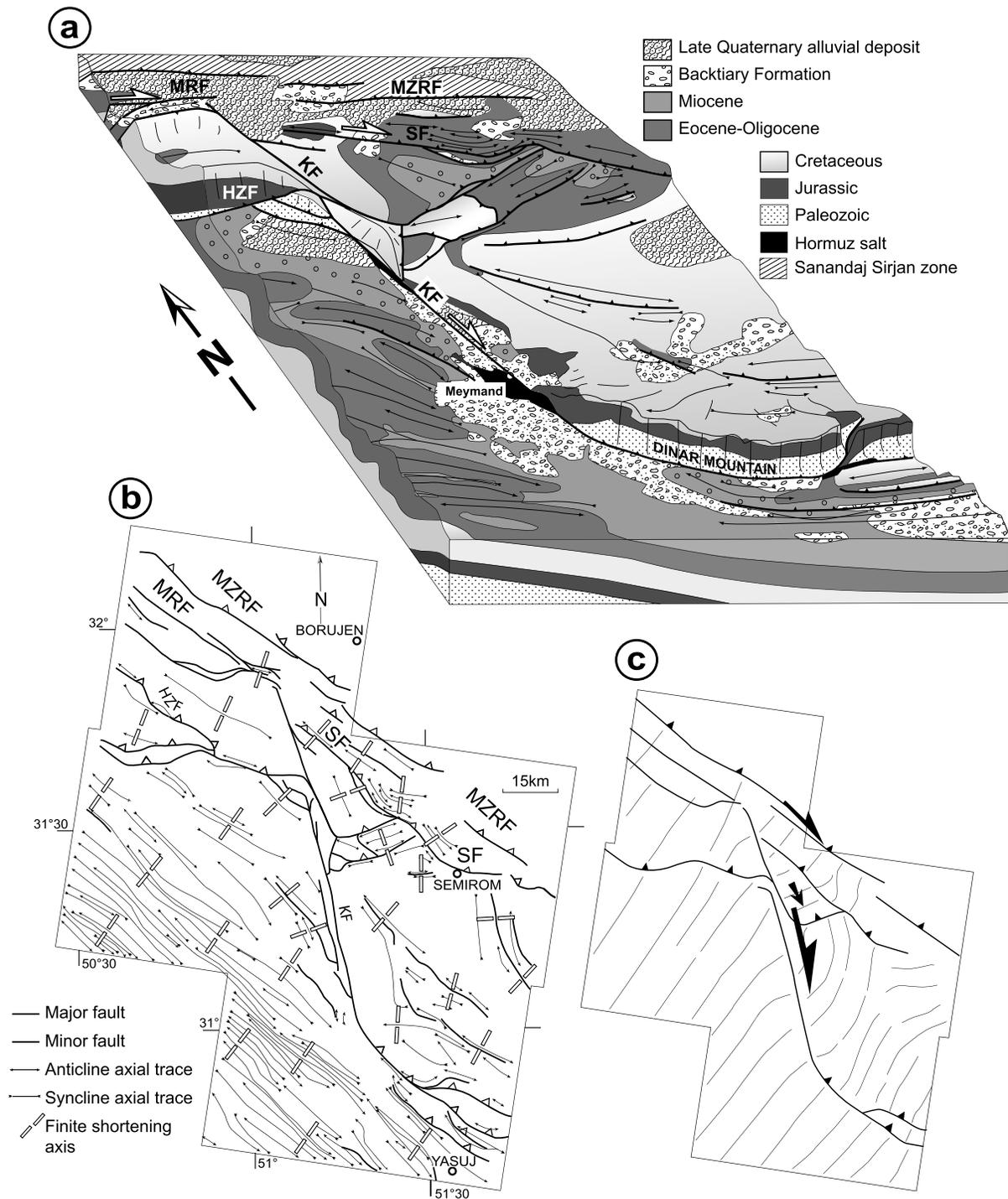
**Figure 8.** Structural geology at the northern tip of the Kazerun Fault. (a) Geological block diagram of the area. Circles in the Miocene indicate conglomeratic facies. (b) Structural map (located on Figure 3). (c) Finite shortening axis trajectories (deduced from fold axes) superimposed on the main structures (same frame as Figure 8b). Figures 8b and 8c are after *Authemayou et al.* [2005]. Information is based on SPOT images interpretation, our field observations, and published geological maps [*Alavi et al.*, 1996; *Sedaghat. et al.*, 1997; *Sedaghat and Shaverdi*, 1997; *Hever*, 1977; *Sedaghat and Gharib*, 1999; *Sedaghat et al.*, 1999; *Ehsanbakhsh Kermani*, 1996].

*Stöcklin*, 1968; *Ricou*, 1976] (Figure 8a). SE verging thrusts and folds of the wedge affect Miocene sediments. They are cut by the Semirom Fault that clearly affects Pliocene sediments (Figure 8a). Two focal mechanisms deduced from microseismicity indicate reverse faulting on E-W striking faults between the KF and the Semirom Fault, to the north of the SE verging thrusts [*Yamini-Fard*, 2003; *Yamini-Fard et al.*, 2006]. The geological map (Figure 8a) also indicates syn- to post-Pliocene activity of the northern KF. It also shows that the MZRF has been active during the Pliocene.

[31] As stated above, the MZRF ceased to be active after activation of the MRF. GPS measurements, our own field geomorphic observations and seismologic data further provide evidence for no significant present-day activity along this fault [*Berberian*, 1981; *Tatar et al.*, 2002; *Yamini-Fard*, 2003; *Yamini-Fard et al.*, 2006]. The northern KF has significant seismic activity with a concentration of earthquakes near the junction between the KF and the MRF, whereas little microseismic activity has been reported from the Semirom Fault [*Yamini-Fard*, 2003; *Yamini-Fard et al.*, 2006] (Figure 4). Focal mechanisms indicate dominant dextral strike-slip faulting along the KF and the southern MRF segment [*Yamini-Fard*, 2003; *Yamini-Fard et al.*, 2006].

### 3.3.2. Tectonic Implication

[32] The deformation pattern of the wedge structural domain is interpreted as a result of the superimposition of SE vergent thrusting/folding and dextral oblique thrusting (from along the Semirom Fault) onto orogen-parallel folds (Figure 8b). Southeastward thrusting on the NE trending reverse faults and the Semirom Fault and strike slip along the northernmost KF took place during at least the Miocene. Strike slip along the KF had already induced reverse dip slip on the Dinar thrust at that time. The SE verging thrusts were later been cut by the Semirom Fault, while strike-slip faulting continued along the KF.

[33] The structural arrangement shown in Figure 8 further implies that the cumulated slip of the two strands of the MRF is transmitted to both the KF and Semirom Fault, at least under the present configuration [*Authemayou et al.*, 2005]. The Semirom Fault absorbs part of the slip from the MRF, while the Kazerun fault zone undergoes dominant right-lateral strike slip and absorbs the remaining part of horizontal strike slip from along the MRF.

[34] These relations suggest a fault pattern rearrangement of the interaction zone between the MRF and the KF similar to that documented further to the northwest in the High Zagros Belt (domains 1 and 2, section 3.1). Indeed, orogen-oblique, SE verging reverse faults that were partly activated together with the northern KF appear to have been abandoned after slip from along the MRF was absorbed by the Semirom Fault and the KF.

## 4.  Fault Kinematics and Stress Regime

[35] In order to constrain the kinematics and stress states along the faults in both space and time, we performed a fault kinematic analysis by inverting the fault slip data (striations) into stress tensor representative of the fault populations.

Inversions have been performed using a computer program derived from the numerical method of *Carey* [1979]. The principles, limitations and applications of the method and derived algorithms for various tectonic environments, especially active settings, are discussed by *Mercier et al.* [1991, and references therein] and *Bellier and Zoback* [1995] [see also *Zoback et al.*, 1989; *Taboada et al.*, 2000; *Garcia et al.*, 2002; *Chang et al.*, 2003; *Siame et al.*, 2005].

[36] Thirty-three sites from the study area (Figure 3) were selected for fault kinematics analyses (Figures 9 and 10). Inversion results (Table 1) include the orientation of the principal stress axes of the computed stress tensor ($\sigma_1$, $\sigma_2$ and $\sigma_3$) and the stress ellipsoid shape parameter $R$, defined as $R = (\sigma_2 - \sigma_1)/(\sigma_3 - \sigma_1)$, which varies from 0 to 1 (see Appendix A).

### 4.1.  Modern Stress Field (Figures 9a and 10)

#### 4.1.1.  Main Recent Fault

[37] Inversions of fault slip data along the MRF indicate a strike-slip regime with an north to NNW trending $\sigma_1$. Stress tensors determined within Paleozoic and Mesozoic rocks from sites 1 and 2 are remarkably consistent with the stress tensors deduced from inversion of data collected within Pliocene to Quaternary sediments at sites 2 and 4). These results may therefore be considered as representative of the faults recent stress regime. Only one station along the MRF (site 5), close to the junction with the KF, records a thrust faulting regime, comparable to that recorded along the MZRF (sites 5 and 6).

#### 4.1.2.  Kazerun Fault

[38] All stress deviators indicate a consistent strike-slip regime along the KF with a thrust-faulting regime around the bent splay fault zone terminations. In an attempt to further constrain the stress state associated with this strike-slip stress regime on a regional scale, we statistically computed the mean principal stress axes from the inversion results on the KF (Figure 9d, left). The mean computed results were then compared to the stress state estimated by inversion of the major representative plane slip data (MFP) selected at each site (Figure 9d, right). Both methods led to consistent results that are in agreement with a regionally significant strike-slip stress regime ($\sigma_2$ vertical) characterized by a N35–40°E trending $\sigma_1$.

#### 4.1.3.  Other Faults

[39] Inversion of fault slip data collected east of the KF within the fan-shaped fault pattern indicate a strike-slip regime characterized by N18°E to N38°E trending $\sigma_1$ and a thrust regime along bent thrust fault terminations. These results are consistent with the stress field around the KF.

[40] Between Kazerun and the Kareh-Bas faults, inversion of fault slip data from a NE trending normal fault bounding an active pull-apart [e.g., *Bachmanov et al.*, 2004] yields a WNW trending $\sigma_3$, consistent with stress tensors obtained on the neighboring faults.

[41] Along the Semirom Fault, inversions of fault slip data indicate a right lateral strike-slip regime associated with a NW trending $\sigma_1$ and a $R$ ratio close to 1 (Table 1). This differs from the NE trending $\sigma_1$ that characterizes the MRF, KF and related faults kinematics.
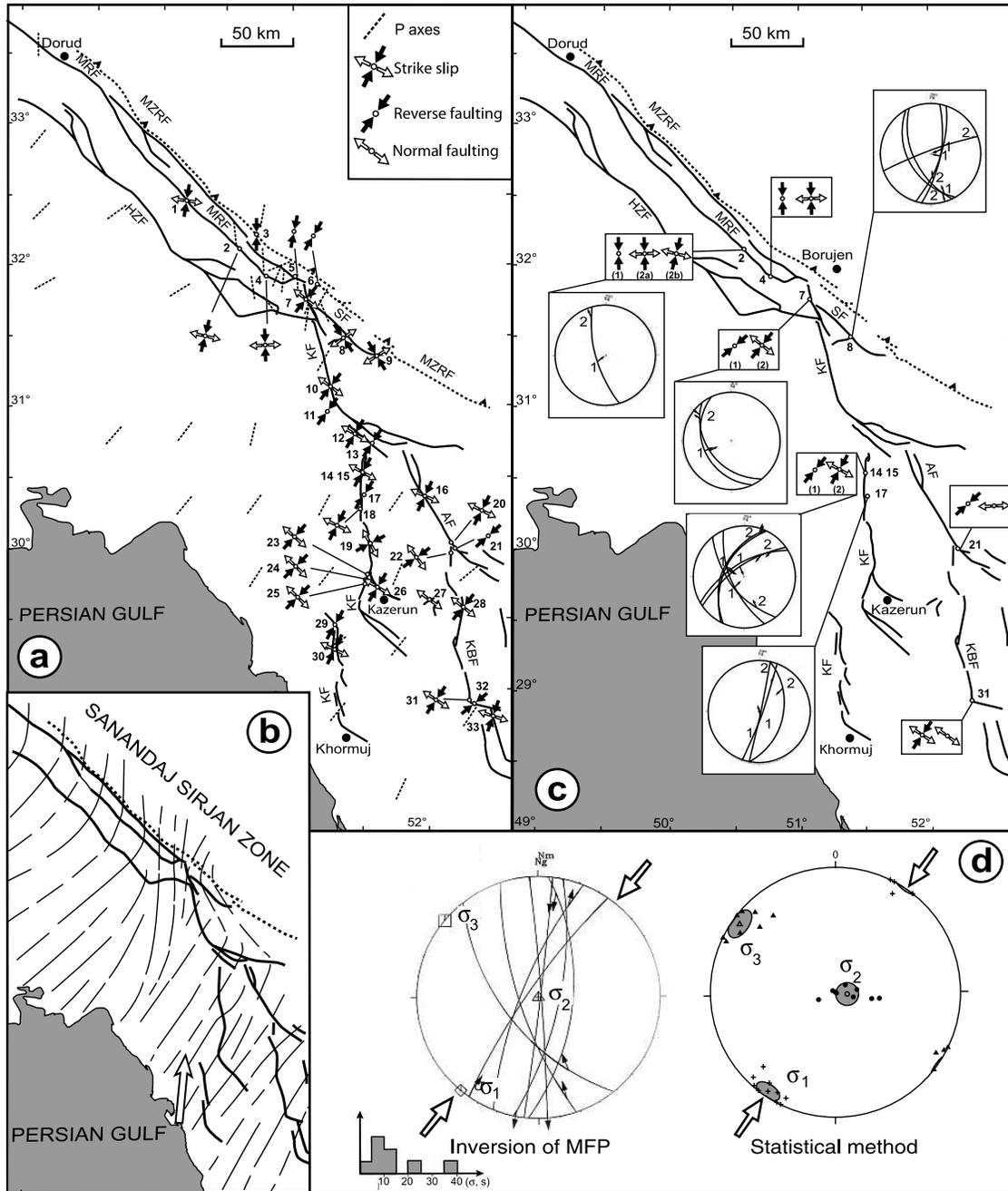
**Figure 9.** Results of fault slip data inversions on the faults of the study area. (a) Modern stress state results. The P axes deduced from local and teleseismic fault plane solutions of earthquake focal mechanisms are compiled after *Vannucci et al.* [2004] and *Yamini-Fard et al.* [2006]. (b) Present-day shortening axis trajectories. White arrow indicates convergence vector with respect to stable Eurasia [*Vernant et al.*, 2004]. (c) Chronology of inversion results. Numbers in parentheses indicate the relative chronology of fault slip data sets. The orientation of the computed principal stress axes defines the stress regimes (i.e., reverse faulting ($\sigma_3$ vertical); normal faulting ($\sigma_1$ vertical) or strike-slip faulting ($\sigma_2$ vertical); Table 1 and Figure 10). Equal angle, lower hemisphere stereonets. Station numbers refer to Table 1. (d) (left) Inversion results for major fault planes striations measured along the Kazerun Fault. (right) Regionally significant mean stress axes computed from a statistical analysis of inversion results along the Kazerun Fault (from sites 7(2), 10, 12, 14 and 15 (2), 20, 23–26, 30). Results are shown with their 95% confidence cones (grey shaded areas) using the McFadden's method computed with PMSTAT software [*Enkin*, 1995].
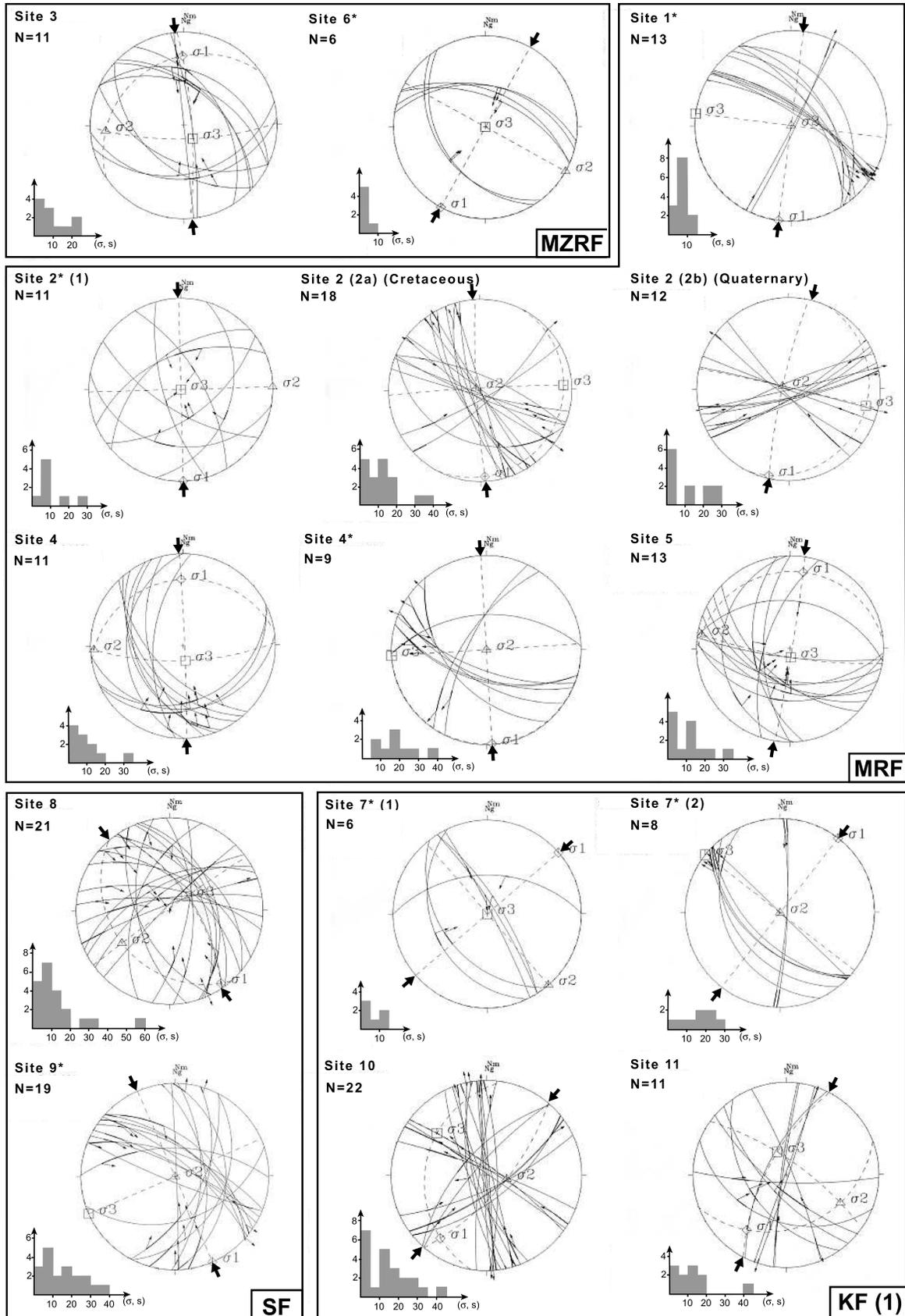
**Figure 10**

#### 4.1.4. Comparison With Earthquake Focal Mechanisms: Summary

[42] In order to obtain a rough picture of the regional recent/current stress field, we have combined P axes deduced from focal mechanisms and the results of fault slip data inversions [e.g., *Chang et al.*, 2003]. P axes and maximum principal stress axes deduced from inversions are coaxial throughout the majority of the study area (Figure 9a). Together with the fact that most of the fault slip data inverted to produce the stress field shown in Figure 9a were measured in Plio-Quaternary sediments, this supports the idea that the computed stress states are representative of the present-day stress field of the study area.

[43] Maximum horizontal stress trajectories are parallel and trend perpendicular to the orogenic trend within the Simple Folded Belt (Figure 9b). They acquire N-S trends along the MRF and NNE trends immediately east of the MRF tip. They trend to the NW in the High Zagros Belt east of the MRF tip, the wedge area of Figure 8, which represents the main zone of interference with an abrupt change in the stress directions (Figure 9b). The stress field is significantly perturbed along the MRF, consistent with partitioning taking place along that fault. Further interference at the southeastern tip of the MRF and at its junction with the fan-shaped fault pattern does not appear to extend into the Simple Folded Belt.

#### 4.2. Stress State Changes

[44] We have distinguished and separated families of striations for 8 of the 33 sites, compatible with two main slip episodes in the fault populations. The discrimination of striae belonging to the two sets was based on a combination of (1) field evidence for slip events cross-cutting relationships on the fault planes and (2) numerical check between incompatible striae and/or with respect with a given stress state. The discrimination of well-defined, distinct families of striations supports the hypothesis of a change in stress regime rather than rotation of fault planes. Along the MRF, KF, and Semirom Fault, this approach has led to the identification of a thrust faulting regime that predates the modern strike-slip regime described above, and is associated with the same directions of maximum principal stress axes.

#### 4.2.1. Timing

[45] Temporal constraints have been taken from along the MRF (Figures 9c and 10). At site 2, Cretaceous limestones and Quaternary fan deposits are brought into contact by the MRF. Fault slip data analysis in the fan provides a single strike-slip regime that is part of the modern regional stress field (site 2b, Figures 9c and Figure 10). Inversions of two distinct sets of slip data in the limestones indicate an early thrust faulting regime (site 1, Figures 9c and 10), and a younger strike-slip regime comparable in directions with the one obtained in the fan deposits (site 2a, Figures 9c and 10). At site 4, the MRF separates Paleozoic rocks from the Plio-Quaternary conglomerates into which the fan deposits described above are stepped (Figure 10). Results obtained from two distinct families of striations measured in the fault breccia were the same as those obtained in the limestone (Figure 9c). This indicates that the change in the stress regime change recorded along the MRF took place during the Pliocene as the earlier thrust fault regime is not recorded in the Quaternary fan deposits.

#### 4.2.2. Extensional Stress States

[46] Along the Kareh-Bas and Ardakan faults, inversions of a separate data set indicate an extensional regime with a NW to west trending $\sigma_3$. This is consistent with the NW trending $\sigma_3$ recorded around the pull apart between the KF and the Kareh-Bas Fault (Figures 9a and 10). Taking into account the lack of relative chronology criteria and the good agreement in the $\sigma_3$ directions of the strike-slip and normal stress regimes, they may be considered as contemporaneous and representative of the modern regional stress field.

## 5. Discussion

[47] This study provides evidence for a reorganization of the fault pattern and kinematic framework of the fold-and-thrust belt during the Pliocene. This change is due to the activation of the MRF at the rear of the fold-and-thrust belt, resulting in a change from dominantly transpressional to partitioned strike-slip deformation in the High Zagros Belt and the abandonment of the MZRF. The onset of slip along the MRF is interpreted to have been accompanied by the regional stress regime change from dominantly thrust slip to right-lateral strike slip documented along the main transcurrent faults of the central Zagros. Within the current kinematic framework, the KF accommodates part of the slip transferred from the MRF and acts as a lateral ramp at the same time. Prior to the activation of the MRF, the KF was most likely already a lateral ramp [*Sepehr and Cosgrove*, 2005].

### 5.1. Kinematic Model

[48] The relations between the MRF, KF, and Semirom faults and the folds and thrusts of the High Zagros Belt further suggest that a large part of the right-lateral slip from along the MRF has been transmitted to the regional fan-

---

**Figure 10.** Fault populations and inversion results of the study area (equal angle, lower hemisphere stereonets). Histograms show the angular deviation (in degree) between the striation (*s*) and the computed shear stress ($\tau$) for each fault plane. Inversions are considered as very well constrained when 80% of the angular deviations are well clustered and below 20°. Asterisks indicate sites for which a fixed inversion method was used, with $\sigma_1$ axis constrained in the horizontal plane (see Appendix A for details). Numbers in parentheses indicate relative chronology of fault slip data sets. Sites are numbered from NW to SE (Figure 9a) and are grouped by faults: MZRF, Main Zagros Reverse Fault; MRF, Main Recent Fault; SF, Semirom Fault; KF, Kazerun Fault; AF, Ardakan Fault; NF, normal faults of the basin located between the Kazerun and Kareh Bas faults; KBF, Kareh Bas Fault.
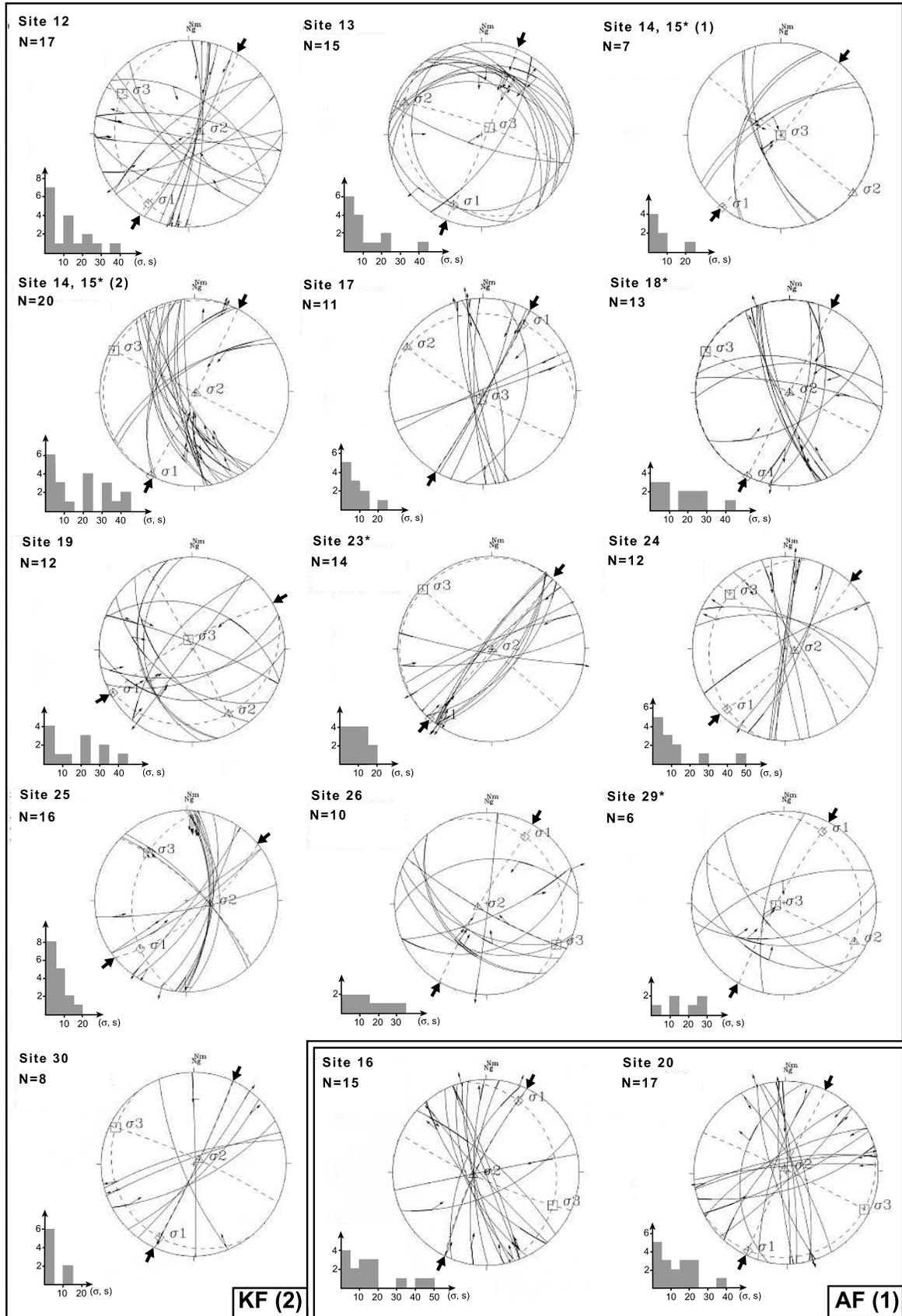
**Figure 10.**   (continued)
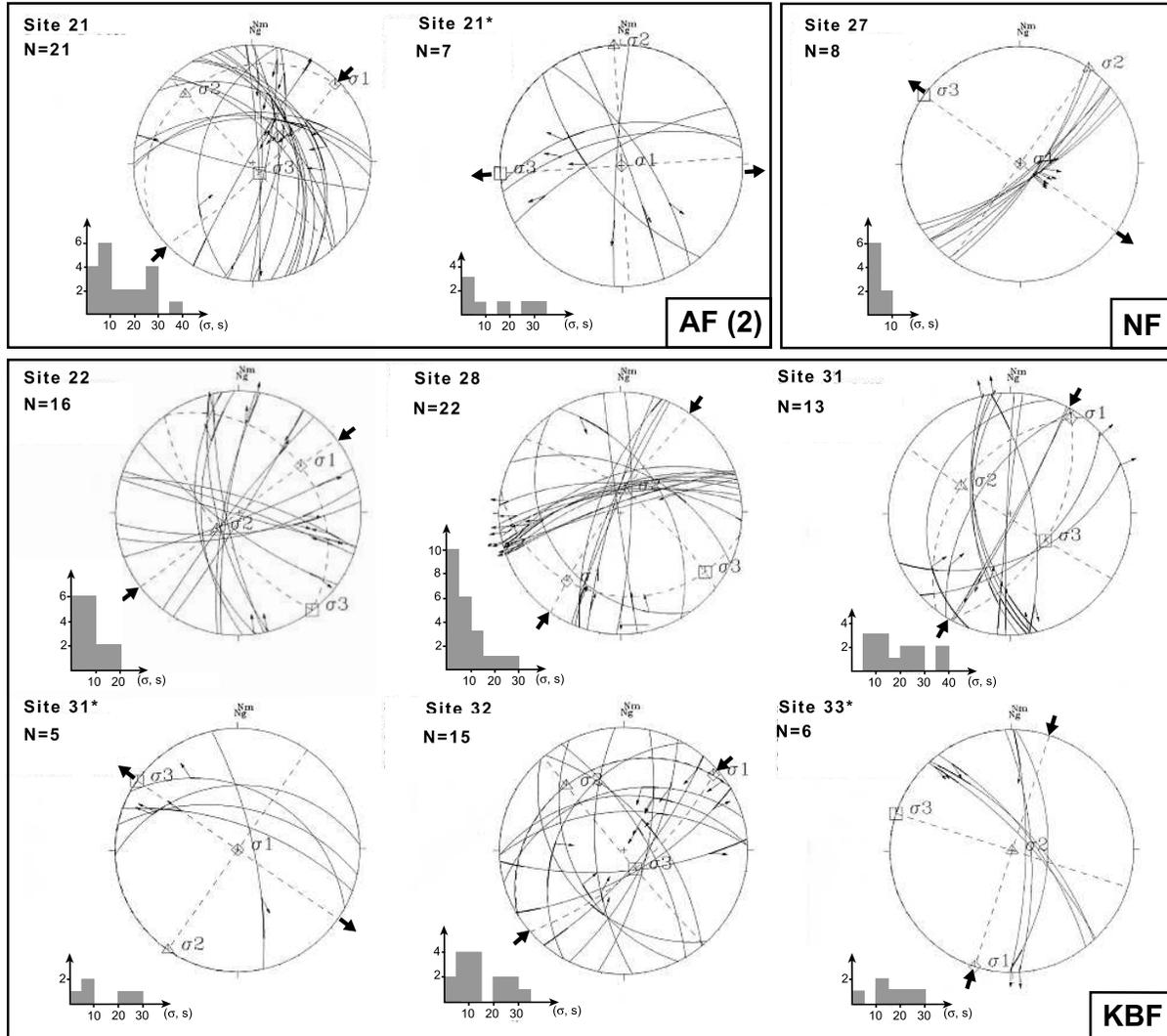
**Figure 10.** (continued)

shaped fault pattern [*Authemayou et al.*, 2005] since the Pliocene kinematic change documented here. We have interpreted this fault pattern to reflect distribution of slip from along the MRF to the fold-and-thrust belt through the thrust terminations of the strike-slip faults of the fan (Figure 11). The Hormuz salt formation assisted slip distribution throughout the belt and permitted the southward migration of the Zagros front, acting as a low-resistance boundary that allowed the extrusion-like process through the fault-shaped pattern produced by transfer of orogen-parallel slip of the MRF to the belt.

[49] Deformation within the fan-shaped fault pattern results from the combination of the effects of right lateral strike-slip along the north to NW trending basement faults of the fan and decoupling along the salt detachment layer. On a large scale, the western limb of the Fars Arc undergoes right-lateral shearing (strengthened by the dextral motion along the faults of the fan) inducing overall clockwise rotation and fold-parallel stretching (Figure 11). This is due to a stronger coupling at the base of the sedimentary

pile toward the NW, i.e., the Hormuz salt formation vanishes against the KF [e.g., *Molinaro et al.*, 2005a]. Stretching, previously suggested by *Baker et al.* [1993] and *Talebian and Jackson* [2004] is confirmed by the extensional stress states derived from fault slip data analyses (Figure 9).

[50] Paleomagnetically derived clockwise rotations along the faults of the fan have been reported [*Aubourg et al.*, 2004; *Bakhtari et al.*, 1998]. However, anticlockwise rotations of the blocks bounded by these same faults should also be considered [*Hessami et al.*, 2001b; *Blanc et al.*, 2003; *Talebian and Jackson*, 2004]. In the vicinity of the strike-slip segments of the KF, including the KF thrust fault zone terminations, a westward increase in reverse displacement on the ramp anticlines suggests anticlockwise rotations of the folds and associated ramps (Figures 7 and 11) [*Bayasgalan et al.*, 1999]. Further, a number of anticline axial trace segments are also left-laterally deflected toward E-W strikes in the vicinity of the north trending dextral strike-slip faults throughout the northwestern part of the

**Table 1.** Results of Stress Tensor Inversions From Fault Slip Data[a]

| Site | Latitude | Longitude | Age and Rock Type | $\sigma_1$ | | $\sigma_2$ | | $\sigma_3$ | | R |
|---|---|---|---|---|---|---|---|---|---|---|
| | | | | Azimuth | Plunge | Azimuth | Plunge | Azimuth | Plunge | |
| 1[b] | 32°22.723′ | 50°11.683′ | Permian dol | 188 | 0 | 20 | 90 | 278 | 0 | 0.15 |
| 2[b] (1) | 32°01.871′ | 50°37.819′ | Cretaceous lim | 178 | 0 | 88 | 0 | 306 | 90 | 0.27 |
| 2 (2a) | 32°01.871′ | 50°37.819′ | Cretaceous lim | 177 | 3 | 298 | 84 | 87 | 5 | 0.68 |
| 2 (2b) | 32°01.871′ | 50°37.819′ | Quaternary alluvial fan | 193 | 2 | 296 | 82 | 103 | 8 | 0.60 |
| 3 | 32°11. 223′ | 50°43. 308′ | Cretaceous ma-lim | 359 | 17 | 266 | 10 | 146 | 70 | 0.92 |
| 4 | 31°57.157′ | 50°43.601′ | Cambrian lim, Plio-Quaternary congl | 358 | 18 | 268 | 2 | 172 | 72 | 0.80 |
| 4[b] | 31°57.157′ | 50°43.601′ | Cambrian lim, Plio-Quaternary congl | 177 | 0 | 357 | 90 | 267 | 0 | 0.00 |
| 5 | 31°54. 941′ | 51°00. 007′ | Plio-Quaternary congl | 10 | 10 | 279 | 2 | 176 | 79 | 0.07 |
| 6[b] | 31°51. 648′ | 51°09. 873′ | Cretaceous marl-lim, Plio-Quaternary congl | 209 | 0 | 119 | 0 | 311 | 90 | 0.28 |
| 7[b] (1) | 31°45. 523′ | 51°05. 747′ | Cretaceous marl-lim | 49 | 0 | 139 | 0 | 317 | 90 | 0.45 |
| 7[b] (2) | 31°45. 523′ | 51°05. 747′ | Cretaceous marl-lim | 38 | 0 | 206 | 90 | 308 | 0 | 0.02 |
| 8 | 31°31.746′ | 51°21.913′ | Miocene congl sandstone, marl | 145 | 3 | 236 | 27 | 49 | 63 | 0.97 |
| 9[b] | 31°24.108′ | 51°39.320′ | Miocene conglomerate sand, marl | 148 | 0 | 58 | 57 | 239 | 33 | 0.63 |
| 10 | 31°07. 457′ | 51°16. 288′ | Jurassic dol | 216 | 11 | 100 | 66 | 311 | 21 | 0.48 |
| 11 | 31°06. 913′ | 51°12. 137′ | Miocene red ma | 215 | 18 | 118 | 23 | 339 | 60 | 0.78 |
| 12 | 30°53. 676′ | 51°23. 014′ | Plio-Quaternary congl | 210 | 8 | 83 | 76 | 302 | 11 | 0.37 |
| 13 | 30°42.571′ | 51°36.119′ | Plio-Quaternary congl | 201 | 11 | 292 | 7 | 52 | 77 | 0.94 |
| 14, 15[b] (1) | 30°27. 425′ 30°33. 002′ | 51°30 931′ 51°30. 578′ | | 219 | 0 | 129 | 0 | 315 | 90 | 0.07 |
| 14, 15[b] (2) | 30°27. 425″ 30°33. 002′ | 51°30 931′ 51°30. 578′ | Oligocene dol | 208 | 0 | 117 | 88 | 298 | 2 | 0.99 |
| 16 | 30°30.103′ | 51°51.236′ | Upper Cretaceous dol | 24 | 10 | 258 | 74 | 117 | 13 | 0.90 |
| 17 | 30°22. 818′ | 51°28. 998′ | Upper Cretaceous lim | 31 | 10 | 300 | 4 | 189 | 80 | 0.96 |
| 18[b] | 30°18. 719′ | 51°30. 147′ | Upper Cretaceous lim | 206 | 0 | 115 | 90 | 296 | 0 | 0.93 |
| 19 | 30°02. 378′ | 51°32. 879′ | Upper Cretaceous lim | 241 | 2 | 151 | 13 | 339 | 77 | 0.97 |
| 20 | 30°16. 467′ | 51°58. 430′ | Upper Cretaceous lim, Oligocene dol | 206 | 3 | 337 | 85 | 116 | 4 | 0.65 |
| 21 | 30°15.110′ | 51°59.554′ | Upper Cretaceous lim | 47 | 2 | 316 | 12 | 146 | 78 | 0.75 |
| 21[b] | 30°15.110′ | 51°59.554′ | Upper Cretaceous lim | 166 | 90 | 357 | 0 | 267 | 0 | 0.20 |
| 22 | 30°14.689′ | 51°58.898′ | Plio-Quaternary congl | 53 | 25 | 233 | 65 | 143 | 0 | 0.35 |
| 23* | 29°49. 261′ | 51°32. 738′ | Oligocene dol, Quaternary congl | 221 | 0 | 131 | 89 | 311 | 1 | 0.98 |
| 24 | 29°46. 882′ | 51°31. 551′ | Miocene dol and ma | 224 | 6 | 105 | 78 | 315 | 10 | 0.11 |
| 25 | 29°45. 862′ | 51°31. 477′ | Miocene dol and ma | 224 | 18 | 98 | 61 | 321 | 22 | 0.80 |
| 26 | 29°41. 007′ | 51°38. 723′ | Quaternary congl | 30 | 10 | 246 | 78 | 121 | 7 | 0.83 |
| 27 | 29°39.430′ | 51°58.467′ | Oligocene dol | 137 | 90 | 36 | 0 | 306 | 0 | 0.81 |
| 28 | 29°29.336′ | 52°10.822′ | Oligocene dol, Quaternary congl | 218 | 19 | 11 | 69 | 125 | 9 | 0.66 |
| 29* | 29°28. 227′ | 51°16. 587′ | Plio-Quaternary conglomerate | 28 | 7 | 119 | 8 | 255 | 79 | 0.25 |
| 30 | 29°16. 403′ | 51°16. 747′ | Oligocene dol, Quaternary congl | 205 | 7 | 53 | 82 | 295 | 4 | 0.51 |
| 31 | 28°57. 288′ | 52°14. 824′ | Oligocene dol | 33 | 4 | 299 | 40 | 127 | 49 | 0.91 |
| 31[b] | 28°57. 288′ | 52°14. 824′ | Oligocene dol | 80 | 90 | 215 | 0 | 305 | 0 | 0.09 |
| 32 | 28°54. 570′ | 52°16. 458′ | Oligocene dol | 50 | 3 | 319 | 20 | 148 | 70 | 0.49 |
| 33[b] | 28°49.767′ | 52°24.008′ | Oligocene dol | 198 | 0 | 101 | 90 | 288 | 0 | 0.81 |

[a]Sites are located on Figure 9 and the corresponding stereograms on Figure 10. Numbers in parentheses indicate relative chronology of distinct fault slip data populations. Lithologies are abbreviated as follows: dol, dolomite; lim, limestone; congl, conglomerate; ma, marl; sand, sandstone.
[b]Sites for which a fixed inversion method was used (see Appendix A for details).

Fars Arc (our own unpublished data, 2005). This indicates that anticlockwise rotations have taken place at least locally along the faults or near fault terminations of the fan.

## 5.2. Specificity of the Fault Pattern

[51] The geometry of the fan-shaped fault pattern and its geometrical and kinematic relationships with the southeastern portion of the MRF suggest the KF and associated faults are second-order faults arranged as a horse-tail like termination of the MRF [*Authemayou et al.*, 2005]. However, the kinematic pattern described here differs from the patterns classically documented at the terminations of large strike-slip fault systems [*Bayasgalan et al.*, 1999], as clockwise rotations have taken place within this dextral strike-slip fault termination. This is due to lateral and vertical decoupling introduced by the Hormuz evaporites within the fold-and-thrust belt. Indeed, clockwise rotation was produced in the
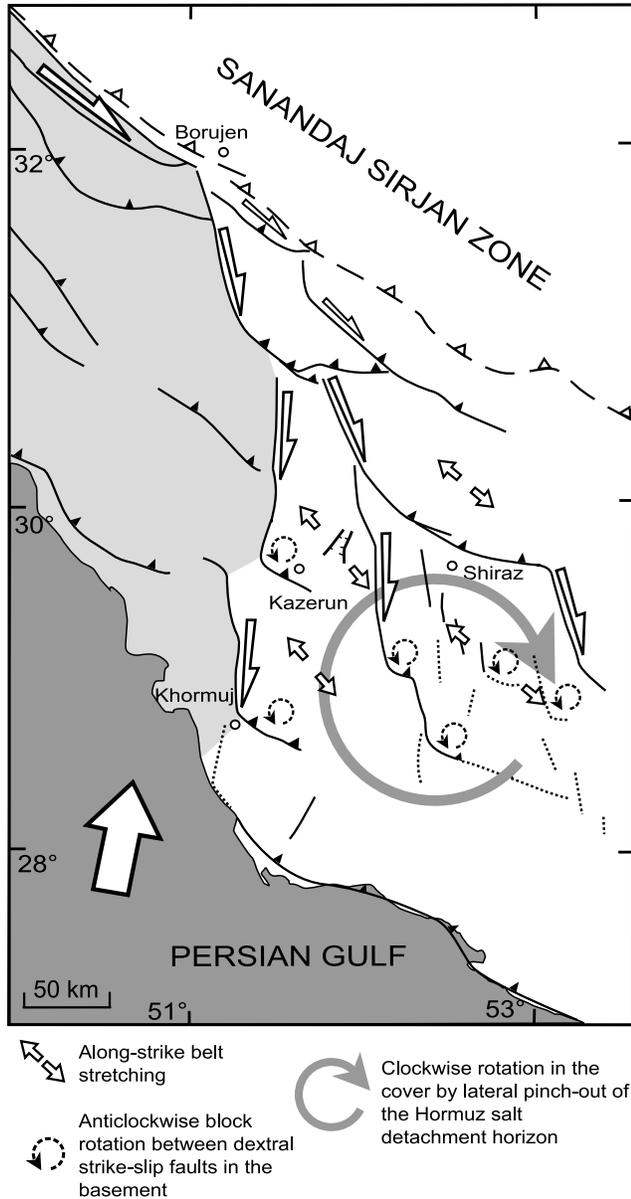
Figure 11. Synthetic kinematic model of the fault system distributing slip of the Main Recent Fault to the Zagros fold-and-thrust belt modified after *Authemayou et al.* [2005]. Dashed lines indicate buried faults [after *Tatar et al.*, 2003; *Blanc et al.*, 2003]. Various rotations about vertical axes and stretching directions are also shown.

cover by a regional dextral shear zone nucleated along the northwestern margin of the salt basin. The combination of (1) vertical decoupling between the cover and its basement, (2) activation of the north to NW trending faults (old inherited basement faults), and (3) detachment and fault-propagation folding further complicated the rotation pattern within the fault termination zone.

[52] This strike-slip fault termination is consistent with the MRF having propagated southeastward within the High

Zagros Belt (possibly from the Bitlis suture zone) until it reached the KF and the Hormuz evaporites. The propagation was stopped by the absorption of slip from along the MRF by the fan-shaped fault pattern. This was facilitated by decoupling along the salt detachment layer, which acted as an almost free boundary allowing (1) south to southeast-ward spreading onto the Arabian platform and (2) stretching of the sedimentary cover together with the activation of the basement right-lateral strike-slip faults and thrusts. Note that most of the faults of the fan, given their orientation with respect to the plate convergence vector, were already active before the activation of the MRF and that the total offset of ~50 km along that fault represents only a small part of the cumulative displacement of the strike-slip faults and thrusts of the northwestern limb of the Fars Arc.

## 5.3. Slip Rate on the Main Recent Fault

[53] The maximum slip rate along the MRF deduced from GPS measurements would be of $4 \pm 2.5$ mm/yr if the fault achieves complete partitioning of the $4-7 \pm 2$ mm/yr of north trending shortening across the western Zagros [*Vernant et al.*, 2004]. This is not in agreement with a Pliocene (3–5 Ma) initiation of the MRF [*Talebian and Jackson*, 2002; this study] and with a cumulative lateral slip of 50 km along that fault, which will lead to a long-term slip rate of 10–17 mm/yr [*Talebian and Jackson*, 2002]. There may be three causes to this, which may have combined resulting in an apparently lower slip rate on the MRF. First, if the cumulative right-lateral offset on the MRF is correct, horizontal slip may still have taken place on the precursor faults to the MRF or in the vicinity of the future MRF between the Late Cretaceous (using the age of the Ophiolite body as an offset marker [*Talebian and Jackson*, 2002]) and the Pliocene, during dominantly transpressive deformation in the High Zagros. Second, the age of the Baktiari Formation, which is essential from establishing the age of the MRF (Figure 5), is underestimated because it is dia-chronous at the scale of the belt. This may therefore need to be refined, at least in the studied area of the High Zagros. Finally, there is a possibility that the slip rate of the MRF has decreased since the Pliocene. Further work is therefore required to assess the slip rate of the MRF in the Quaternary by examining the displacement of dated Quaternary geo-morphic features.

## 5.4. Tectonic Cause(s) and Consequences of Kinematic Change

[54] Our fault kinematics analysis is in agreement with the results of *Regard et al.* [2004] who documented a regional change from reverse to transpressional faulting pattern in the southeasternmost Zagros that they attributed to the Pliocene. This kinematic change may also be linked to the transition from thin-skinned to thick-skinned and out-of-sequence thrusting recognized in the eastern Zagros, which would also be of Pliocene age [*Molinaro et al.*, 2005a].

[55] The onset of partitioning along the MRF cannot have resulted from a change in the convergence obliquity because the convergence vector has remained relatively stable over

the last 80 Ma [*Savostin et al.*, 1986; *McQuarrie et al.*, 2003; *Vernant et al.*, 2004]. *Talebian and Jackson* [2002] attributed this event to the reorganization of the Arabia-Eurasia collision at 5 ± 2 Ma [*Westaway*, 1994; *Allen et al.*, 2004]. Evidence for this event is has been found in the rapid uplift of the Alborz Mountains [*Axen et al.*, 2001], an increase of the south Caspian Sea subsidence [*Allen et al.*, 2002], the onset of spreading in the Red sea [*Joffe and Garfunkel*, 1987], and the final closure of marginal basins that formed central Iran [*Berberian and King*, 1981; *McCall*, 1996].

[56] According to *Westaway* [2003], the large variation of sea level during the Messinian salinity crisis may have changed the state of stress in the eastern Mediterranean region. However, *Allen et al.* [2004] have suggested that the cause for this reorganization was the shift of crustal shortening away from the thicker crustal region of Turkey-Iranian plateau and Greater Caucasus, resulting in increased buoyancy forces. The cause for this shift is debated. *Molinaro et al.* [2005b] have suggested that the downgoing Arabian lithospheric slab breakoff and consecutive thermal uplift of the Iranian plateau may be the cause of the involvement of basement fault activity. Slab detachment, by increasing the coupling between the two plates, could further favor partitioning along a newly formed fault such as the MRF. Further, deformation along the MRF could be localized by a thermally softened zone under the suture zone caused by an increased regional geothermal gradient resulting from the slab breakoff.

[57] Surface waveform tomography [e.g., *Maggi and Priestley*, 2005] and lithospheric-scale geometric modeling [*Molinaro et al.*, 2005b] suggest the presence of a thin lithosphere and warm upper mantle beneath the Zagros suture zone and the Turkish-Iranian plateau. These results, together with the lack of seismic evidence for active subduction beneath the Iranian plateau [*Talebian and Jackson*, 2004], support the removal of the mantle lithosphere generally associated with slab breakoff.

[58] By combining geological observations and analog modeling, *Faccenna et al.* [2006] have shown that collision reorganization could result from slab breakoff. They propose that slab breakoff triggered the change in the kinematic regime in Turkey, which implies the acquisition of a coherent plate motion and the onset of more steady state westward tectonic escape of the Anatolian plate during early Pliocene [*Reilinger et al.*, 1997]. This would be associated with westward propagation of the North Anatolian Fault and formation of the current main strand of the East Anatolian Fault in the early Pliocene (∼5 Ma) and late early Pliocene (∼3 Ma), respectively [e.g., *Saraǧlu et al.*, 1992; *Bozkurt*, 2001; *Şengör et al.*, 2005]. Contemporaneously, a change in the faulting regime, basin type and deformation pattern (from folding and thrusting to strike-slip faulting) occurred in the vicinity of the eastern Anatolia triple junction (Figure 1) [*Koçyiğit et al.*, 2001].

[59] A potential symmetric effect may be envisaged with a southeastward propagation of the MRF accompanying propagation of the Bitlis suture zone slab breakoff to the southeast, at the time of initiation of slip along the North Anatolian Fault. The complete partitioning along the MRF may have been set up at the time of formation of the East Anatolian Fault, accompanied with the late Pliocene kinematic change. The current regional stress regime was incipient during the late Pliocene and became fully active afterward.

## 6. Conclusion

[60] The present analysis provides constraints for the kinematic reconstruction of a key region for understanding the accommodation of the Eurasia-Arabia oblique convergence. A two-step kinematics scenario is proposed involving the transition from a distributed transpressional regime located at the rear of the Zagros fold-and-thrust belt, to partitioning of oblique convergence along the newly formed MRF.

[61] Until the early Pliocene, deformation was accommodated through a ∼50-km-wide transpressional belt (i.e., the High Zagros Belt) with high-angle imbricate thrust faults. Later in the Pliocene, the strike-slip partitioned motion of oblique plate convergence became achieved by strike slip along the MRF. Since that time, slip from along the MRF is transmitted and distributed southeastward into the thrusts and folds of the Zagros through a fan-shaped fault network made of the KF and associated faults. This fault system corresponds to an orogen-scale horse-tail, strike-slip fault termination of the MRF. The youth of the MRF may suggest that this current fault configuration represents a transient step of the southeastward propagation of the MRF.

## Appendix A: Methodology of Inversion of Fault Plane Populations

[62] The inversion method assumes that the striation ($s$) occurs in the direction of the resolved shear stress (the tangential stress, i.e., the projection of the applied stress on the fault plane) on each fault plane, the fault plane being the preexisting fracture. Inversion computes a mean best fitting deviatoric stress tensor from a set of striated faults by minimizing the angular deviation between a predicted slip vector (maximum shear, $\tau$) and the observed striation ($s$) [*Carey*, 1979; *Angelier*, 1984; *Mercier et al.*, 1991]. The method supposes that rigid block displacements are independent. Inversion results include the orientation (azimuth and plunge) of the principal stress axes of a mean deviatoric stress tensor as well as a stress ellipsoid shape parameter $R = (\sigma_2 - \sigma_1)/(\sigma_3 - \sigma_1)$, where $\sigma_1$, $\sigma_2$, and $\sigma_3$, correspond to the compressional, intermediate and extensional principal stress axes, respectively.

[63] In a strike-slip regime, the $R = 0$ end-member corresponds to a stress state transitional to normal faulting (transtensional regime; $\sigma_2$ or $\sigma_1$ vertical and $\sigma_2$ close to $\sigma_1$ in magnitude); whereas the $R = 1$ end-member represents a stress state transitional to thrust faulting (transpressional regime; $\sigma_2$ or $\sigma_3$ vertical and $\sigma_2$ close to $\sigma_3$ in magnitude). For $R$ values close to 0 or to 1, the near-transitional (i.e., near uniaxial when $0.85 < R < 1$ and $0 < R < 0.15$) stress

states require only minor fluctuation of stress magnitudes to go from a strike-slip to a compressional regime or extensional regime, respectively. Thus such regimes are characterized by mixed modes of faulting: dip, oblique, and strike slip.

[64] Inversion results are generally considered reliable if 80% of the angular deviations between $\tau$ and $s$ are less than 20°. Ideal sets of data contain faults dipping in two directions with distinct strike directions. For poorly distributed fault sets (e.g., data sets that contain faults with few distinct strike directions and dipping in both directions) a "fixed" inversion is used [*Bellier and Zoback*, 1995], in which the principal stress axes are fixed to lie in horizontal and vertical planes. In that case, only two independent fault sets are sufficient to compute a solution. The computed horizontal stress orientations from the fixed inversion are generally within 5–10° of the stress axes obtained from standard inversion although the fixed

inversion results may be characterized by unstable and unconstrained $R$ values. In the present case, many of the fixed inversions yield results similar to that of standard inversion of higher quality data sets on the same fault zone (Figures 9 and 10).

## References

Agard, P., J. Omrani, L. Jolivet, and F. Mouthereau (2005), Convergence history across Zagros (Iran): Constraints from collisional and earlier deformation, *Int. J. Earth Sci.*, *94*, 401–419.

Alavi, M. (1994), Tectonics of the Zagros orogenic belt of Iran: New data and interpretations, *Tectonophysics*, *229*, 211–238.

Alavi, M., I. Nayai, M. Yousefi, M. E. Segaghat, and B. Hanzepour (1996), Geological map of Iran, Borujen sheet, scale 1:250,000, Geol. Surv. of Iran, Tehran.

Allen, M. B., S. Jones, A. Ismail-Zadeh, M. D. Simmons, and L. Anderson (2002), Onset of subduction as the cause of rapid Pliocene-Quaternary subsidence in the south Caspian Basin, *Geology*, *30*, 775–778.

Allen, M. B., J. Jackson, and R. Walker (2004), Late Cenozoic re-organization of the Arabia-Eurasia collision and the comparison of short-term and long-term deformation rates, *Tectonics*, *23*, TC2008, doi:10.1029/2003TC001530.

Angelier, J. (1984), Tectonics analysis of slip data sets, *J. Geophys. Res.*, *89*, 5835–5848.

Aubourg, C., B. Smith, H. Bakhtari, N. Guya, A. Eshragui, S. Lallemant, J.-C. Guezou, M. Molinaro, X. Braud, and S. Delaunay (2004), Post-Miocene shortening direction pictured by magnetic fabric across the Zagros-Makran syntaxis, *Spec. Pap. Geol. Soc. Am.*, *383*, 17–40.

Authemayou, C., O. Bellier, D. Chardon, Z. Malekzade, and M. Abbassi (2005), Role of the Kazerun fault system in active deformation of the Zagros fold-and-thrust belt (Iran), *C. R. Geosci.*, *337*, 539–545.

Axen, G. J., P. S. Lam, M. Grove, D. F. Stockli, and J. Hassanzadeh (2001), Exhumation of the western-central Alborz Mountains, Iran, Caspian subsidence in the South Caspian Basin, and collision related tectonics, *Geology*, *29*, 559–562.

Bachmanov, D. M., V. G. Trifonov, K. T. Hessami, A. I. Kozhurin, T. P. Ivanova, E. A. Rogozhin, M. C. Hademi, and F. H. Jamali (2004), Active faults in the Zagros and central Iran, *Tectonophysics*, *380*, 221–241.

Baker, C., J. Jackson, and K. Priestley (1993), Earthquakes on the Kazerun line in the Zagros Mountains of Iran: Strike-slip faulting within a fold-and-thrust belt, *Geophys. J. Int.*, *115*, 41–61.

Bakhtari, R. H., D. Frizon de Lamotte, C. Aubourg, and J. Hassanzadeh (1998), Magnetic fabrics of Tertiary sandstones from the Arc of Fars (eastern Zagros, Iran), *Tectonophysics*, *284*, 299–316.

Bayasgalan, A., J. Jackson, J.-F. Ritz, and S. Carretier (1999), Field examples of strike-slip fault termina-

tions in Mongolia and their tectonic significance, *Tectonics*, *18*, 394–411.

Bellier, O., and M. Zoback (1995), Recent state of stress change in the Walker Lane zone, western Basin and Range province, United States, *Tectonics*, *14*, 564–593.

Berberian, M. (1981), Active faulting and tectonics of Iran, in *Zagros, Hindu Kush, Himalaya, Geodynamic Evolution*, *Geodyn. Ser.*, vol. 3, edited by H. K. Gupta and F. M. Delany, pp. 33–69, AGU, Washington, D. C.

Berberian, M. (1995), Master blind thrust faults hidden under the Zagros folds: Active basement tectonics and surface morphotectonic, *Tectonophysics*, *241*, 193–224.

Berberian, M., and G. C. P. King (1981), Towards a paleogeography and tectonic evolution of Iran, *Can. J. Earth Sci.*, *18*, 210–285.

Berthier, F., J. P. Billiault, B. Halbronn, and P. Maurizot (1974), Etude stratigraphique, pétrologique et structurale de la région de Khorramabad (Zagros central), Ph.D. thesis, 181 pp., Univ. Joseph Fourier, Grenoble, France.

Blanc, E. J.-P., M. B. Allen, S. Inger, and H. Hassani (2003), Structural styles in the Zagros Simple Folded Zone, Iran, *J. Geol. Soc. London*, *160*, 401–412.

Bozkurt, E. (2001), Neotectonics of Turkey: A syntesis, *Geodin. Acta*, *14*, 3–30.

Braud, J. (1970), Les formations du Zagros dans la région de Kermanshah (Iran) et leurs rapports structuraux, *C. R. Acad. Sci.*, *271*, 1241–1244.

Carey, E. (1979), Recherche des directions principales de contraintes associées au jeu d'une population de failles, *Rev. Geol. Dyn. Geogr. Phys.*, *21*, 57–66.

Chang, C.-P., T.-Y. Chang, J. Angelier, H. Kao, J.-C. Lee, and S.-B. Yu (2003), Strain and stress field in Taiwan oblique convergent system: Constraints from GPS observation and tectonic data, *Earth Planet. Sci. Lett.*, *214*, 115–127.

Ehsanbakhsh Kermani, M. H. (1996), Geological quadrangle map of Iran, Ardal sheet, sheet 6153, scale 1:100,000, Geol. Surv. of Iran, Tehran.

Enkin, R. J. (1995), A computer Program Package for Analysis and Presentation of Paleomagnetic data-PMSTAT, Pac. Geosci. Cent., Geol. Surv. Can., Sydney, B. C.

Faccenna, C., O. Bellier, J. Martinod, C. Piromallo, and V. Regard (2006), Slab detachment beneath eastern Anatolia: A possible cause for the formation of the North Anatolian Fault, *Earth Planet. Sci. Lett.*, *242*, 85–97.

Falcon, N. L. (1969), Problem of the relationship between surface structures and deep displacement illustrated by the Zagros range, in *Time and Place in Orogeny*, edited by P. E. Kent, G. E. Satterwaite, and A. M. Spencer, *Geol. Soc. Spec. Publ.*, *3*, 9–22.

Falcon, N. L. (1974), Southern Iran: Zagros Mountains, in *Mesozoic-Cenozoic Orogenic Belts, Data for Orogenic Studies*, edited by A. M. Spencer, *Geol. Soc. Spec. Publ.*, *4*, 199–211.

Garcia, S., J. Angelier, F. Bergerat, and C. Homberg (2002), Tectonic analysis of an oceanic transform fault zone based on fault-slip data and earthquake focal mechanism: The Husavk-Flatey Fault zone, Iceland, *Tectonophysics*, *344*, 157–174.

Gidon, M., F. Berthier, J.-P. Billiault, B. Halbronn, and P. Maurizot (1974a), Sur les caractères et l'ampleur du coulissement de la "Main Fault" dans la région de Borudjerd-Dorud (Zagros oriental, Iran), *C. R. Acad. Sci.*, *278*, 701–704.

Gidon, M., F. Berthier, J.-P. Billiault, B. Halbronn, and P. Maurizot (1974b), Sur quelques caractères de la tectonique néocrétacée dans la région de Borudjerd (Zagros oriental, Iran), *C. R. Acad. Sci.*, *278*, 577–580.

Gidon, M., F. Berthier, J.-P. Billiault, B. Halbronn, and P. Maurizot (1974c), Charriage et mouvements sinsédimentaires tertiaires dans la région de Borudjerd (Zagros, Iran), *C. R. Acad. Sci.*, *278*, 421–424.

Hajmolla-ali, A., A. M. Hosseini, M. B. Farhadian, and E. Sedaghat (1991), Geological map of Iran, Borujen sheet, sheet 5757, scale 1:100,000, Geol. Surv. of Iran, Tehran.

Haynes, S. J., and H. McQuillan (1974), Evolution of the Zagros Suture Zone, southern Iran, *Geol. Soc. Am. Bull.*, *85*, 739–744.

Hessami, K., H. A. Koyi, C. J. Talbot, H. Tabasi, and E. Shabanian (2001a), Progressive unconformities within an evolving foreland fold-thrust belt, Zagros Mountains, *J. Geol. Soc. London*, *158*, 969–981.

Hessami, K., H. A. Koyi, and C. J. Talbot (2001b), The significance of strike-slip faulting in the basement of the Zagros fold and thrust belt, *J. Petrol. Geol.*, *24*, 5–28.

Hever, H. J. (1977), Geological map of Iran, Behbehan-Gachsaran sheet, sheet 20511, scale 1:250,000, Natl. Iran. Oil Co., Tehran.

Homke, S., J. Vergés, L. Garcés, H. Emani, and R. Karpuz (2004), Magnetostratigraphy of Miocene-Pliocene Zagros foreland deposits in the front of the Push-e Kush Arc (Lurestan Province, Iran), *Earth Planet. Sci. Lett.*, *225*, 397–410.

Jackson, J. A. (1992), Partitioning of strike-slip and convergent motion between Eurasia and Arabia in eastern Turkey and Caucasus, *J. Geophys. Res.*, *97*, 12,471–12,479.

Jackson, J. A., and D. P. McKenzie (1988), The relationship between plate motion and seismic moment tensors, and the rates of active deformation in the Mediterranean and Middle East, *Geophys. J. R. Astron. Soc.*, *93*, 45–73.

Joffe, S., and Z. Garfunkel (1987), Plate kinematics of the circum Red Sea: A re-evaluation, *Tectonophysics*, *141*, 5–22.

Koçyiğit, A., A. Yilmaz, S. Adamia, and S. Kulosshvili (2001), Neotectonics of East Anatolian Plateau (Turkey) and Lesser Caucasus: Implication for transition from thrusting to strike-slip faulting, *Geodin. Acta*, *14*, 177–195.

Koop, W. J., and R. Stoneley (1982), Subsidence history of the Middle East Zagros Basin, Permian to recent, *Philos. Trans. R. Soc. London, Ser. A*, *305*, 149–168.

Maggi, A., and K. Priestley (2005), Surface waveform tomography of the Turkish-Iranian plateau, *Geophys. J. Int.*, *160*, 1068–1080.

McCall, G. J. H. (1996), The inner Mesozoic to Eocene ocean of south and central Iran and associated microcontinents, *Geotectonics*, *29*, 490–499.

McQuarrie, N., J. M. Stock, C. Verdel, and B. P. Wernicke (2003), Cenozoic evolution of Neotethys and implications for the causes of plate motions, *Geophys. Res. Lett.*, *30*(20), 2036, doi:10.1029/2003GL017992.

Mercier, J.-L., E. Carey-Gailhardis, and M. Sébrier (1991), Paleostress determinations from fault kinematics: Application to the Neotectonics of the Himalayas-Tibet and the central Andes, *Philos. Trans. R. Soc. London*, *337*, 41–52.

Mohajjel, M., and C. L. Fergusson (2000), Dextral transpression in Late Cretaceous continental collision, Sanandaj-Sirjan Zone, western Iran, *J. Struct. Geol.*, *22*, 1125–1139.

Mohajjel, M., C. L. Fergusson, and M. R. Sahandi (2003), Cretaceous-Tertiary convergence and continental collision, Sanandaj-Sirjan Zone, western Iran, *J. Asian Earth Sci.*, *21*, 397–412.

Molinaro, M., P. Letrumy, J.-C. Guezou, D. Frizon de Lamotte, and S. A. Eshraghi (2005a), The structure and kinematics of the south-eastern Zagros fold-thrust belt, Iran: From thin-skinned to thick-skinned tectonics, *Tectonics*, *24*, TC3007, doi:10.1029/2004TC001633.

Molinaro, M., H. Zeyen, and X. Laurencin (2005b), Lithospheric structure underneath the south-eastern Zagros Mountains, Iran: Recent slab break-off?, *Terra Nova*, *17*, 1–6.

Pattinson, R., and M. Takin (1971), Geological significance of the Dezful embayement boundaries, Rep. 1166, Natl. Iran. Oil Co., Tehran.

Regard, V., O. Bellier, J.-C. Thomas, M. R. Abbassi, J. L. Mercier, E. Shabanian, K. Feghhi, and S. Soleymani (2004), The accommodation of Arabia-Eurasia convergence in the Zagros-Makran transfer zone, SE Iran: A transition between collision and subduction through a young deforming system, *Tectonics*, *23*, TC4007, doi:10.1029/2003TC001599.

Reilinger, R. E., S. C. McClusky, M. B. Oral, R. W. King, M. N. Toksoz, A. A. Barka, I. Kinik,

O. Lenk, and I. Sanli (1997), Global Positioning System measurements of present-day crustal movements in the Arabia-Africa-Eurasia plate collision zone, *J. Geophys. Res.*, *102*, 9983–9999.

Ricou, L. E. (1976), Evolution structurale des Zagrides, la région clef de Neyriz (Zagros Iranien), *Mem. Soc. Geol. Fr.*, *55*, 1–140.

Sarağlu, F., Ö. Emre, and I. Kuşçu (1992), The East Anatolian Fault of Turkey, *Ann. Tectonicae*, *6*, 125–199.

Savostin, L. A., J.-C. Sibuet, L. P. Zanenshain, X. Le-Pichon, and M.-J. Roulet (1986), Kinematic evolution of the Tethys belt from the Atlantic Ocean to the Pamirs since the Triassic, *Tectonophysics*, *123*, 1–35.

Sedaghat, M. E., and F. Gharib (1999), Geological map of Iran, Dena sheet, sheet 6948, scale 1:100,000, Geol. Surv. of Iran, Tehran.

Sedaghat, M. E., and T. Shaverdi (1997), Geological map of Iran, Sisakht sheet, sheet 6251, scale 1:100,000, Geol. Surv. of Iran, Tehran.

Sedaghat, M. E., M. Usefi, E. Kavari, and I. Navai (1997), Geological map of Iran, Borujen sheet, sheet 6253, scale 1:100,000, Geol. Surv. Min. Expl., Tehran.

Sedaghat, M. E., F. Gharib, and T. Shaverdi (1999), Geological map of Iran, Semirom sheet, sheet 6352, scale 1:100,000, Geol. Surv. of Iran, Tehran.

Şengör, A. M. C., O. Tüysüz, C. İmren, M. Sakinç, H. Eyidoğan, N. Görür, X. Le Pichon, and C. Rangin (2005), The North Anatolian Fault: A new look, *Annu. Rev. Earth Planet. Sci.*, *33*, 37–112.

Sepehr, M., and J. W. Cosgrove (2004), Structural framework of the Zagros Fold-and-Thrust Belt, Iran, *Mar. Petr. Geol.*, *21*, 829–843.

Sepehr, M., and J. W. Cosgrove (2005), Role of the Kazerun Fault zone in the formation and deformation of the Zagros Fold-Thrust Belt, Iran, *Tectonics*, *24*, TC5005, doi:10.1029/2004TC001725.

Sherkati, S., and J. Letouzey (2004), Variation of structural style and basin evolution in the central Zagros (Izeh zone and Dezful Embayment), Iran, *Mar. Petr. Geol.*, *21*, 535–554.

Siame, L. L., O. Bellier, M. Sébrier, and M. Araujo (2005), Deformation partitioning in flat subduction setting: Case of the Andean foreland of western Argentina (28°S–33°S), *Tectonics*, *24*, TC5003, doi:10.1029/2005TC001787.

Stöcklin, J. (1968), Structural history and tectonics of Iran, A review, *AAPG Bull.*, *52*, 1229–1258.

Stöcklin, J. (1974), Possible ancient continental margins in Iran, in *The Geology of Continental Margins*, edited by C. A. Burke and C. L. Drake, pp. 873–877, Springer, New York.

Stoneley, R. (1981), The geology of the Kuh-e Dalneshin area of southern Iran, and its bearing on the evolution southern Tethys, *J. R. Soc. London*, *138*, 509–526.

Taboada, A., L. A. Rivera, A. Fuenzalida, A. Cisternas, P. Hervé, H. Bijwaard, J. Olaya, and C. Rivera (2000), Geodynamics of the northern Andes: Subductions and intracontinental deformation (Colombia), *Tectonics*, *19*, 787–813.

Talbot, C. J., and M. Alavi (1996), The past of a future syntaxis across the Zagros, in *Salt Tectonics*, edited by G. I. Alsop, D. J. Blundell, and I. Davison, *Geol. Soc. Spec. Publ.*, *100*, 89–110.

Talebian, M., and J. Jackson (2002), Offset on the Main Recent Fault of the NW Iran and implications for the late Cenozoic tectonics of the Arabia-Eurasia collision zone, *Geophys. J. Int.*, *150*, 422–439.

Talebian, M., and J. Jackson (2004), A reappraisal of earthquake focal mechanisms and active shortening in the Zagros Mountains of Iran, *Geophys. J. Int.*, *156*, 506–526.

Tatar, M., D. Haztfeld, J. Martinod, A. Walpersdorf, M. Ghafori-Ashtiany, and J. Chéry (2002), The present-day deformation of the central Zagros from GPS measurements, *Geophys. Res. Lett.*, *29*(19), 1927, doi:10.1029/2002GL015427.

Tatar, M., D. Haztfeld, and M. Ghafori-Ashtiany (2003), Tectonics of the central Zagros (Iran) deduced from microearthquake seismicity, *Geophys. J. Int.*, *156*, 255–266.

Tchalenko, J. S., and J. Braud (1974), Seismicity and structure of Zagros (Iran): The Main Recent Fault between 33° and 35°N, *Philos. Trans. R. Soc. London*, *277*, 1–25.

Vannucci, G., S. Pondrelli, A. Argnani, A. Morelli, P. Gasperini, and E. Boschi (2004), An atlas of Mediterranean seismicity, *Ann. Geophys.*, *47*, 247–326.

Vernant, P., et al. (2004), Contemporary crustal deformation and plate kinematics in Middle East constrained by GPS measurements in Iran and northern Oman, *Geophys. J. Int.*, *157*, 381–398.

Westaway, R. (1994), Present-day kinematics of the Middle East and eastern Mediterranean, *J. Geophys. Res.*, *99*, 12,071–12,090.

Westaway, R. (2003), Kinematics of the Middle East and eastern Mediterranean updated, *Turk. J. Earth Sci.*, *12*, 5–46.

Yamini-Fard, F. (2003), Sismotectonique et structure lithosphérique de 2 zones de transition dans le Zagros (Iran): La zone de Minab et la zone de Qatar-Kazerun, Ph.D. thesis, pp. 208, Univ. Joseph Fourier, Grenoble, France.

Yamini-Fard, F., D. Hatzfeld, M. Tatar, and M. Mokhtari (2006), Microseismicity on the Kazerun fault system (Iran): Evidence of a strike-slip shear zone and a thick crust, *Geophys. J. Int.*, in press.

Yilmaz, Y. (1993), New evidence and model on the evolution of the southeast Anatolian orogen, *Geol. Soc. Am. Bull.*, *105*, 251–271.

Zahedi, M., M. Rahmati Ilkhchi, and J. Vaezipour (1993), Geological map of Iran, Shahrekord sheet, sheet E8, scale 1:250,000, Geol. Surv. of Iran, Tehran.

Zoback, M. L., et al. (1989), Global patterns of tectonic stress, *Nature*, *341*, 291–298.

———————————
M. R. Abbassi and Z. Malekzadeh, International Institute of Earthquake Engineering and Seismology, Sholeh str., 8th Kohestan, Pasdaran, Tehran, Iran.

C. Authemayou, O. Bellier, and E. Shabanian, Centre Européen de Recherche et d'Enseignement de Géosciences de l'Environnement (UMR CNRS 6635), Université Paul Cézanne, BP 80, 13545, Aix-en-Provence Cedex 4, France. (authemayou@cerege.fr)

D. Chardon, Institut de Recherche pour le Développement, UMR 161-CEREGE, BP A5, 98848 Nouméa Cedex, New Caledonia.